Performance of Orthogonal and Non-Orthogonal TH-PPM for Multi-User UWB Communication Systems

by

Behzad Bahr-Hosseini
B.Sc., University of Arak, Iran, 2003

A Thesis Submitted in Partial Fulfillment of the
Requirements for the Degree of

MASTER OF APPLIED SCIENCE

in the Department of Electrical and Computer Engineering

Performance of Orthogonal and Non-Orthogonal TH-PPM for Multi-User UWB Communication Systems

by

Behzad Bahr-Hosseini
B.Sc., University of Arak, Iran, 2003

Supervisory Committee

Dr. T. Aaron Gulliver, Co-Supervisor
(Dept. of Electrical and Computer Engineering)

Dr. Wei Li, Co-Supervisor
(Dept. of Electrical and Computer Engineering)

Dr. Abolfazl Ghassemi, Departmental Member
(Dept. of Electrical and Computer Engineering)

Supervisory Committee

Dr. T. Aaron Gulliver, Co-Supervisor
(Dept. of Electrical and Computer Engineering)

Dr. Wei Li, Co-Supervisor
(Dept. of Electrical and Computer Engineering)

Dr. Abolfazl Ghassemi, Departmental Member
(Dept. of Electrical and Computer Engineering)

ABSTRACT

The performance of orthogonal pulse position modulation (PPM) and non-orthogonal pulse position modulation (NPPM) is studied and compared with different ultra wideband (UWB) channel models. Time hopping (TH) is used to decrease the effect of interference in multi access environments. Rake receiver is studied as an ideal UWB receiver for multiuser environments. It is shown that an ideal rake (I-Rake) receiver has the best performance among all rake receivers, followed by 5 finger selective rake (5S-Rake), 5 finger partial rake (5P-Rake), 2 finger selective rake (2S-Rake), and 2 finger partial rake (2P-Rake). With a large number of users, NPPM can achieve a better bit error rate (BER) performance than PPM. It is also shown that PPM and NPPM in a triple Saleh-Valenzuela (TSV) channel has performance similar to that in a Saleh-Valenzuela (SV) channel.

Contents

List of Tables

List of Figures

List of Abbreviations

2P-Rake	2-finger Partial Rake
2S-Rake	2-finger Selective Rake
5P-Rake	5-finger Partial Rake
5S-Rake	5-finger Selective Rake
Ant	Antenna
AoA	Angle of Arrival
AWGN	Additive White Gaussian Noise
BER	Bit Error Rate
CDMA	Code Division Multiple Access
CIR	Channel Impulse Response
DoD	Department of Defense
DS	Direct Sequence
DVD	Digital Video Disc
EIRP	Equivalent Isotropically Radiated Power
FCC	Federal Communications Commission
Gbps	Gigabits per Second
GHz	Gigahertz
GPS	Global Positioning System
I-Rake	Ideal Rake
Int	Interferer
IR	Impulse Response
IEEE	Institute of Electrical and Electronics Engineers
ISI	Inter Symbol Interference
LOS	Line of Sight
Mbps	Megabits per Second
MHz	Megahertz
ML	Maximum Likelihood
MM-Wave	Millimeter Wave
MRC	Maximum Ratio Combining
NLOS	Non Line of Sight

NPPM	Non-orthogonal Pulse Position Modulation
PAM	Pulse Amplitude Modulation
pdf	Probability Density Function
PDP	Power Delay Profile
PG	Processing Gain
PN	Pseudo-random Noise
PPAM	Pulse Position Amplitude Modulation
PPM	Pulse Position Modulation
PR	Pseudo Random
PSD	Power Spectral Density
RF	Radio Frequency
RFID	Radio Frequency Identification
RMS	Root Mean Square
RX	Receiver
SNR	Signal to Noise Ratio
SV	Saleh-Valenzuela
TG3a	IEEE802.15.3a Task Group
TG3c	IEEE802.15.3c Task Group
TH	Time Hopping
ToA	Time of Arrival
TSV	Triple-SV
TX	Transmitter
UWB	Ultra Wideband
WHDMI	Wireless High Definition Multimedia Interface
WLAN	Wireless Local Area Network
WPAN	Wireless Personal Area Network
WUSB	Wireless Universal Serial Bus

List of Symbols

a_q	Data Symbol
A	Shadowing Path Loss
b_i	Input Bits
B	Channel Bandwidth
B_f	Fractional Bandwidth
c	Speed of Light
C	Channel Capacity
C_i	Random Code
d	Distance
d_1	Direct Path
d_2	Reflected Path
D	Distance Between Transmit and Receive Antennas
f	Frequency
f_c	Center Frequency
f_H	Higher Frequency
f_L	Lower Frequency
G	Gain
G_t	Transmitter Antenna Gain
G_{t1}	Transmitter Gain for Direct Path
G_{t2}	Transmitter Gain for Reflected Path
G_r	Receiver Antenna Gain
G_{r1}	Receiver Gain for Direct Path
G_{r2}	Receiver Gain for Reflected Path
G_{TX}	Maximum Transmitter Antenna Gain
h_1	Transmit Antenna Height
h_2	Receive Antenna Height
$h(t)$	Channel Impulse Response
$I(t)$	Interference

$j_i(t)$	Basis Function
$j(t-\tau)$	Cross Correlator Basis Function
J	Number of Different Waveforms
K	Constant
L_I	All Multipath Components
L_P	Partial Multipath Components
L_S	Selective Multipath Components
m	Ray Number
M	Total Number of Rays
n	Cluster Number
$n(t)$	Noise
N	Total Number of Clusters
N_s	Number of Pulses Per Bit
P_{nm}	Uniform Random Variable with value from ± 1
P_r	Received Signal Power
$p(t)$	Pulse
P_t	Transmitted Signal Power
P_B	Bit Error Probability
P_{Noise}	Noise Power
P_{TX}	Maximum Transmitter Antenna Power
q	Bit Number
Q	Total Number of Bits
$r(t)$	Received Signal
R_b	Bit Rate
$s_j(t)$	Waveform
s_{ji}	Correlator Function
$s(t)$	Transmitted Signal
s_{OOK}	OOK Signal
s_{PAM}	PAM Signal
s_{PPM}	PPM Signal
S	Signal Power
t	Time
T	Pulse Repetition
T_c	Chip Duration
T_f	Frame Time
T_n	First Ray Arrival Time
T_p	Pulse Duration
U	Total Number of Users

$\sqrt{W}$	Signal Amplitude
$\sqrt{W_{RX}}$	Received Signal Amplitude
$\sqrt{W_{TX}}$	Transmitted Signal Amplitude
$\sqrt{W^{(u)}}$	Amplitude of the uth User
Z	Decision Variable
Z_n	Decision Variable for Noise
Z_I	Decision Variable for Interference
Z_{RX}	Decision Variable for Received Signal
α	Channel Gain
α_{nm}	Multipath Gain Coefficient of the m-th Ray in the n-th Cluster
β_{nm}	Lognormal Fading Term
χ	Antenna Beam Width
$\delta()$	Dirac Delta Function
ϵ	PPM Shift
γ	Ray Power Decay
Γ	Cluster Power Decay
Γ_0	Reflection Coefficient
λ	Ray Arrival Rate
λ_f	Wavelength of Center Frequency
Λ	Cluster Arrival Rate
μ_D	Average Distance Distribution
μ_{nm}	Mean
$\rho(\epsilon)$	Autocorrelation Function
σ^2	Variance
σ_ϕ	Ray Angle Spread
τ	Channel Delay
$\tau_{n,(m-1)}$	Delay of the $(m-1)$-th Ray in the n-th Cluster
Ω_0	Average Power of the First Ray of the First Cluster
Ψ_n	AoA of the n-th cluster
ψ_{nm}	AoA of the m-th ray in the n-th cluster
ζ_n	Channel Gain Fluctuations on each Cluster
ζ_{nm}	Channel Gain Fluctuations on each Ray within a Cluster

ACKNOWLEDGEMENTS

This thesis could not have been accomplished without the assistance of many people whose contributions I gratefully acknowledge.

Foremost, I would like to express my sincere gratitude toward my graduate advisor Professor T. Aaron Gulliver for his continuous support, excellent academic advice and his input since the beginning of the study. I deeply appreciate his visionary supervision and constructive suggestions in numerous ways during the course of this thesis.

I would like to thank my co-supervisor Dr. Wei Li for giving his insightful advice which shaped my unformed ideas to start the thesis.

I want to express my gratitude to Dr. Abolfazl Ghassemi for his guidance throughout my thesis. Without the degree of support that I got from him, this thesis could not have been successfully completed.

I would like to thank my many student colleagues in our Telecommunications lab for providing a stimulating and fun environment in which to learn and grow, specially my good friend Carlos Quiroz Perez for all the support, entertainment, and caring he provided.

I wish to thank my family who always supported me by their unwavering love and encouragement. My sisters Bahareh, Kathy and Mercedeh, and my aunt Mitra.

I wish to thank my family in Victoria for providing a loving environment for me. My uncle, Abie, aunty, Nahid, cousins, Tahara and Ian, and Farid. I have been lucky to have them.

Lastly, and most importantly, I wish to thank my parents, Azar and Mohammad. They raised me, supported me, taught me, and loved me. To them I dedicate this thesis.

DEDICATION

This thesis is dedicated to my parents for their love, endless support and encouragement.

Chapter 1

Introduction

In recent years demand for faster, less expensive and more secure wireless communications has increased remarkably. The entrance of new technologies to the wireless world has made the radio frequency spectrum over crowded, which results in higher prices for spectrum licensing and lower availability of spectrum. Ultra wideband (UWB) [1], [2] is one solution to the spectrum concerns. UWB devices work under the noise floor and therefore can coexist with the other technologies with very little interference [3]. The noise like nature of UWB signals results from the allocation of a significantly large bandwidth for this technology. Therefore, UWB is capable of offering very large data rates, in the order of gigabits per second (Gbps), which makes this technology very attractive.

Another reason that makes UWB attractive in the wireless market is that a vast number of applications can use UWB. The trade-off between data rate and distance is the reason for the diversity of applications. UWB can transfer information with a very high data rate, but over a short range, or with a lower data rate but over a longer range. This can be done by using more pulses per bit, which lowers the data rate but allows for a longer transmission distance [4].

1.1 UWB History and FCC Regulations

The first use of impulse radio goes back to 1901 when Guglielmo Marconi used Morse code to transfer information. He used a spark gap radio transmitter to send data over the Atlantic Ocean. About sixty years later, the US military started using impulse radio because it is an extremely secure transmission technique. For almost thirty years,

from the 1960's to 1990 research was almost exclusively done by the US Department of Defence (DoD). In the recent years, due to advances in fast semiconductors impulse radio has made its way into commercial applications under the new name of UWB. In February 2002, federal communications commission (FCC) [5] allowed for unlicensed commercial use of UWB for high data rate short range wireless data communications [3].

Based on the FCC definition, UWB signals must have bandwidth of at least 500MHz or a fractional bandwidth of at least 0.20. The fractional bandwidth is defined as [5]

$$B_f = \frac{B}{f_c} \times 100 = \frac{(f_H - f_L)}{(f_H + f_L)/2} \times 100 \tag{1.1}$$

where B and f_c are the total UWB bandwidth and center frequency, respectively, and f_H and f_L are the higher and the lower frequencies at -10 dB.

The initial FCC spectrum allocation for the use of unlicensed UWB is 7.5 GHz between 3.1 GHz and 10.6 GHz. All UWB devices operating in this frequency range must limit their effective isotropic radiated power (EIPR) to below -41.3 dBm/MHz or 75 nW/MHz [5]. EIRP specifies the maximum power that an UWB transmitter is allowed to transmit and is given by

$$EIRP = P_{TX}.G_{TX} \tag{1.2}$$

where P_{TX} and G_{TX} are the maximum power and gain of the transmitter antenna. The FCC power restrictions for indoor and outdoor UWB communications are shown in Figs. 1.1 and 1.2, respectively. The EIRP for some other UWB applications namely, vehicular radar, and (low, mid and high) frequency imaging are shown in Table 1.1.

Frequency Band (GHz)	0.96-1.61	1.61-1.99	1.99-3.1	3.1-10.6	10.6-22.0
LowFreq. Imaging EIRP (dBm/MHz)	-65.3	-53.3	-51.3	-51.3	-51.3
MidFreq. Imaging EIRP (dBm/MHz)	-53.3	-51.3	-41.3	-41.3	-51.3
HighFreq. Imaging EIRP (dBm/MHz)	-65.3	-53.3	-51.3	-41.3	-51.3
Vehicular Radar EIRP (dBm/MHz)	-75.3	-61.3	-61.3	-61.3	-61.3

Table 1.1: FCC Spectral Masks for UWB Applications.

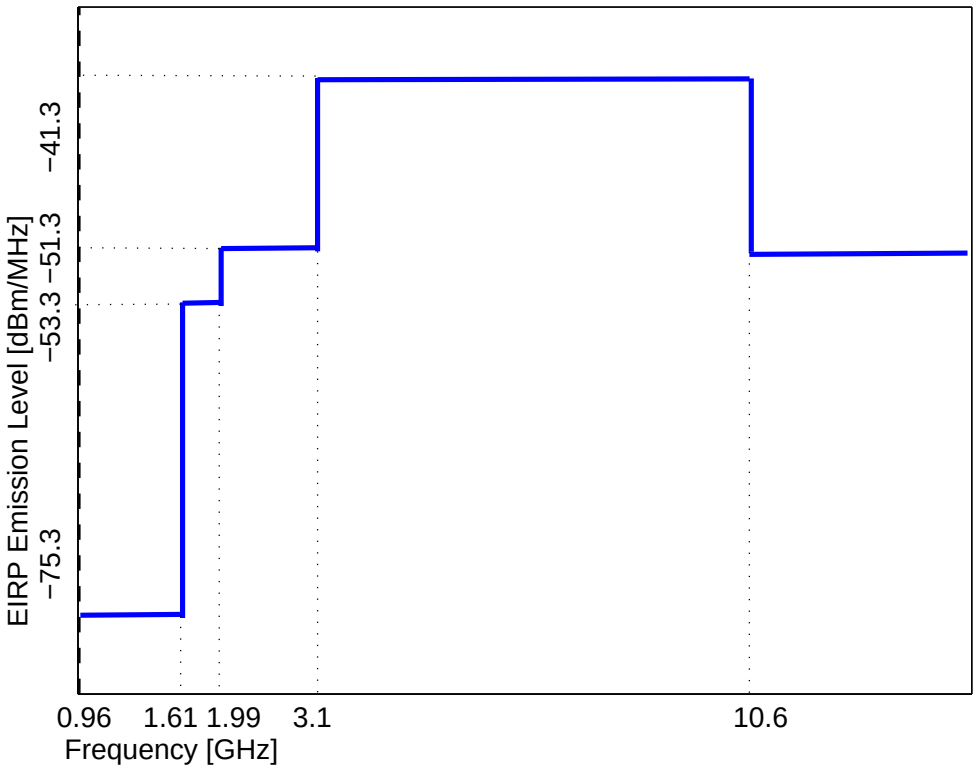

Figure 1.1: FCC spectral mask for indoor UWB communications.

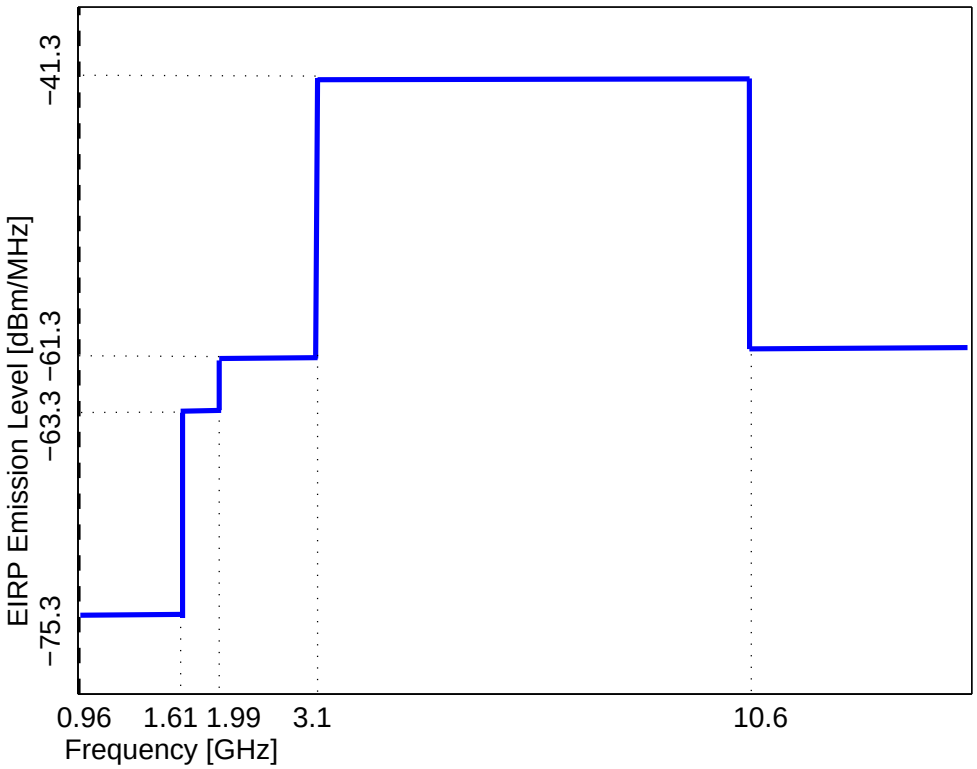

Figure 1.2: FCC spectral mask for outdoor UWB communications.

1.2 UWB Concept

Ultra wideband communications spreads the total signal power across a very wide band of frequencies up to 7.5 GHz within the region 3.1 GHz to 10.6 GHz. This wide band can be obtained using very short duration pulses, resulting in a signal with a very low power spectral density (PSD). This reduces the interference to narrowband users that use the same spectrum, while yielding a low probability of detection and excellent multipath immunity. The low probability of interference comes from the fact that the very low PSD appears as noise to other systems because the UWB signal is below their noise floors. UWB also has a very low duty cycle which results in a very low average transmission power. The duty cycle is the actual time duration of the pulse over the time when a pulse can be transmitted [3].

1.3 UWB Advantages

UWB has several advantages over narrow band systems. The first advantage is the low complexity of this system. This is due to the carrierless nature of UWB signal which eliminates several radio frequency (RF) components from the circuit, such as local oscillators and complex delay and phase tracking loops [4]. The unlicensed bandwidth eliminates expensive licensing fees and bandwidth costs. UWB can share the spectrum with other systems because signal can be generated which are below the noise floor of other users [4]. This also decreases the probability of detection which results a higher security for UWB systems.

As mentioned previously, due to the low pulse duty cycle, UWB has a low average transmission power. This low power translates into the longer battery life for UWB devices which can be an important advantage.

A high data rate is another advantage of UWB, but this can be achieved only for short range communications. The high data rate is a result of the large bandwidth and thus large channel capacity as given by Shannon's theorem [6]

$$C = B \log_2 \left(1 + \frac{S}{P_{noise}} \right) \tag{1.3}$$

where C, B, S and P_{noise} are the channel capacity, channel bandwidth, total signal power and total noise power, respectively. Since UWB has a very large bandwidth, the channel capacity which defines the maximum bit rate, is very large.

UWB systems have greater resistance to jamming compared with narrow band systems. The reason is that these systems have a high processing gain (PG) [3], which is given by $PG = \frac{RFBandwidth}{DataBandwidth}$. The processing gain can be interpreted as frequency diversity, which provides resistance to jamming.

Finally, UWB has a better performance in multipath channels with multiple users compared with narrow band systems. The very short duration of transmitted pulses is the reason for this, as the nanosecond duration pulses are unlikely to overlap [3].

1.4 UWB Challenges

Some of the challenges exist for UWB communication are, UWB pulse distortion, complicated synchronization between the receiver and the transmitter and complicated channel estimation.

According to the Friis formula

$$P_r = P_t \cdot G_t \cdot G_r(c/(4\pi df))^2. \tag{1.4}$$

P_r, P_t, G_t and G_r are the received and transmitted signal powers and the transmitter and receiver antenna gains, respectively; c, d and f are the speed of light, transmitter and receiver distance and the signal frequency. It can be seen in the equation that with increase of frequency, the received signal power decreases. Due to the very wide range of UWB frequencies the received power changes constantly and as a result the pulse shape gets distorted [3].

The other challenge is the synchronization of high frequency UWB transmitter and receiver. Due to the very short duration of UWB pulses, the sampling and synchronization is more complicated than narrow band. To overcome this, very fast analog to digital converters are required [3].

Moreover, because of the wide frequency band of UWB and the reduced signal energy, channel estimation would also be a complicated task [3].

1.5 60 GHz MM-Wave Communications

While having all the advantages the lower frequency UWB band has over narrow band systems, this frequency band, although approved by the FCC, is not available in all countries. Therefore, the entire 7.5 GHz of bandwidth cannot be used globally

[7]. In addition, the capacity in this band is insufficient for some applications such as coaxial cable replacement in the home [7]. Finally, even though lower frequency UWB signals are below the noise floor and this reduces the interference to the other systems, some interference still occurs, i.e., the UWB signal introduces additional noise to other systems.

The frequency range of 57 GHz to 64 GHz, the 60 GHz millimeter-wave (mm-wave) [8] band, is another frequency range that has been made available for UWB communications. This frequency range is a promising solution for all the aforementioned problems. 3.5 to 7 GHz of bandwidth is available worldwide over the 60 GHz frequency band, as summarized in Fig. 1.3 [9]. Due to the high frequency and large bandwidth, 60 GHz mm-wave can support data rates up to 2-3 Gbps [8]. Also mm-wave signals do not interfere with other systems as much since fewer systems operate at these higher frequencies. This higher frequency band operation can be seen to provide higher security for mm-wave systems.

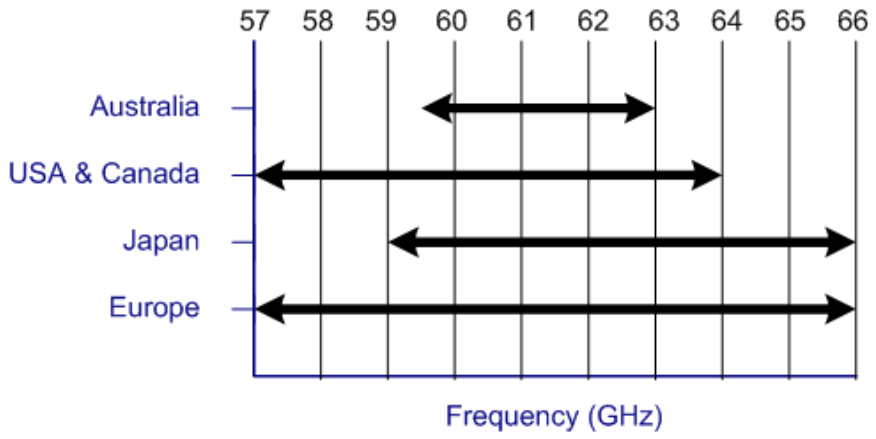

Figure 1.3: Available global frequency bands around 60 GHz.

A higher frequency band means greater path loss for the transmitted signal. Furthermore, in this frequency range, atmospheric phenomena such as oxygen (O_2) absorption exists. Oxygen absorption is absorption of electromagnetic energy by oxygen molecules. The resulting severe attenuation of mm-wave signals can be overcome by using multiple directional antennas. Other advantages of this approach are higher spatial reuse, higher security and less interference to other users [8]. Challenges with this channel inlcude increased transceivers phase noise and limited gain amplifiers [7].

The advantages and disadvantages of lower UWB band and mm-wave UWB systems are shown in Tables 1.2 and 1.3.

UWB Benefits	UWB Challenges
Low complexity	Pulse shape distortion
Low interference	complicated synchronization
Coexistance with narrow band	complicated channel estimation
High security	
Low power and long battery life	
High date rate	
No licence fee	
Resistance to jamming	
Better performance in multipath environments	

Table 1.2: UWB advantages and disadvantages compared to narrow band communications.

60 GHz mm-wave UWB Benefits	60 GHz mm-wave UWB Challenges
Frequency band available globaly	Greater pathloss
High capacity (cable replacement)	Oxygen absorption
Less interference	Transceiver phase noise
Higher security	Limited gain amplifiers
High spatial reuse	

Table 1.3: 60 GHz UWB advantages and disadvantages compared to lower frequency UWB.

1.6 UWB Pulse Modulation Schemes

High data rate impulse radio UWB provides short range communications with very low transmitted power, and can be implemented simply. It uses a pulse or a sequence of pulses which are amplitude and/or position modulated. One of the simplest types of modulation used in UWB communications is on-off keying (OOK) [10]. This modulation uses the presence or absence of a pulse to modulate the binary data sequence. Fig. 1.4 shows that the presence of a pulse represents bit "1", and the absence of a pulse represents bit "0". The OOK signal is given by

$$s_{OOK} = \sum_{q=0}^{Q-1} a_q p(t - qT) \tag{1.5}$$

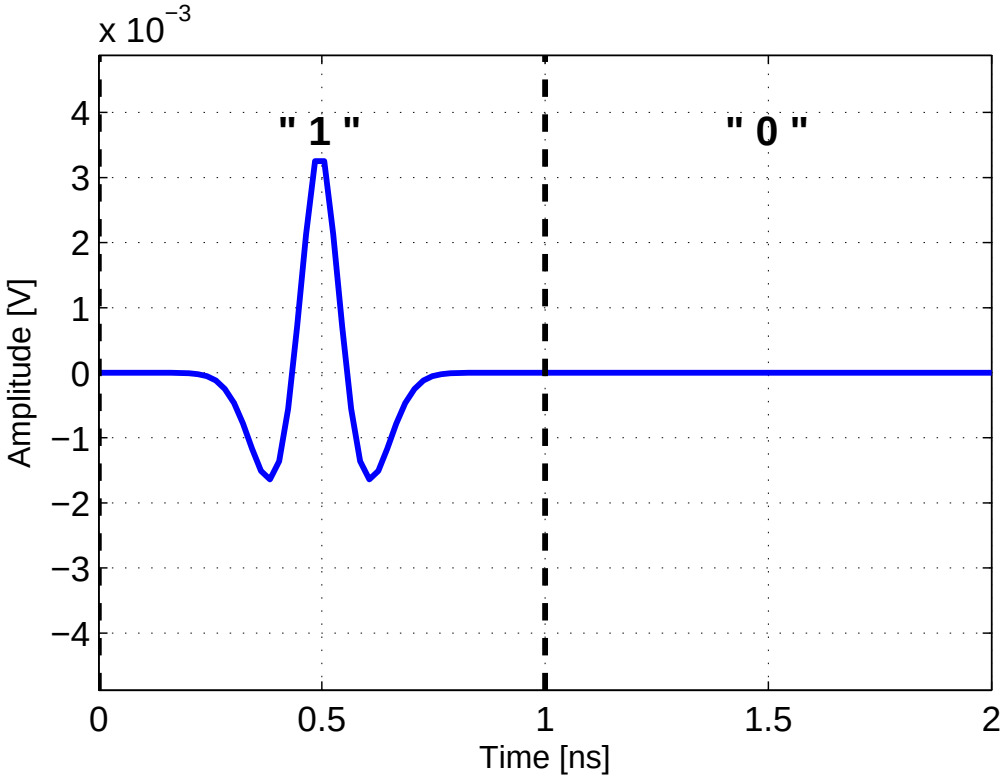

Figure 1.4: On-off keying modulation.

where Q, T, $p(t)$, and a_q are total number of bits, pulse repetition, pulse, and data symbol given by

$$a_q = \begin{cases} 0 & \text{represents bit “0”} \\ 1 & \text{represents bit “1”} \end{cases}.$$

During off times there is no transmission, and as a result undesired signals may be detected as a transmitted signal. This can cause poor performance in multiple access environments.

An improved form of this modulation is pulse amplitude modulation (PAM) [11], where the amplitude is varied according to the data. Antipodal PAM modulation is shown in Fig. 1.5, where “1” and “0” are represented by two different signal polarities. PAM modulation can be modeled using(1.5) but with different symbol representations

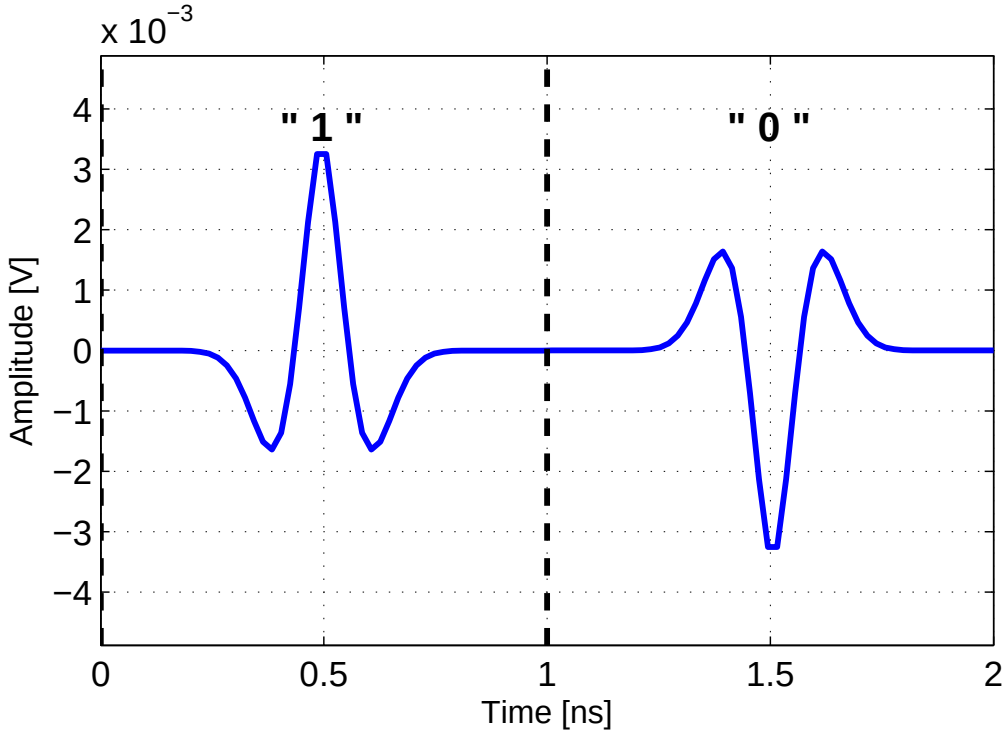

Figure 1.5: Antipodal PAM modulation.

given by $a_q = \begin{cases} -1 & \text{represents bit “0”} \\ 1 & \text{represents bit “1”} \end{cases}$.

PAM performs better than OOK at the cost of higher complexity due to the second (negative) pulse. The complexity can be reduced by using pulse position modulation (PPM) [11], in which case the position of the pulse is determined by the data. PPM modulation is illustrated in Fig. 1.6, where a pulse with no shift represents bit “0”,

and a shifted pulse represents bit "1". The PPM modulation can be shown by

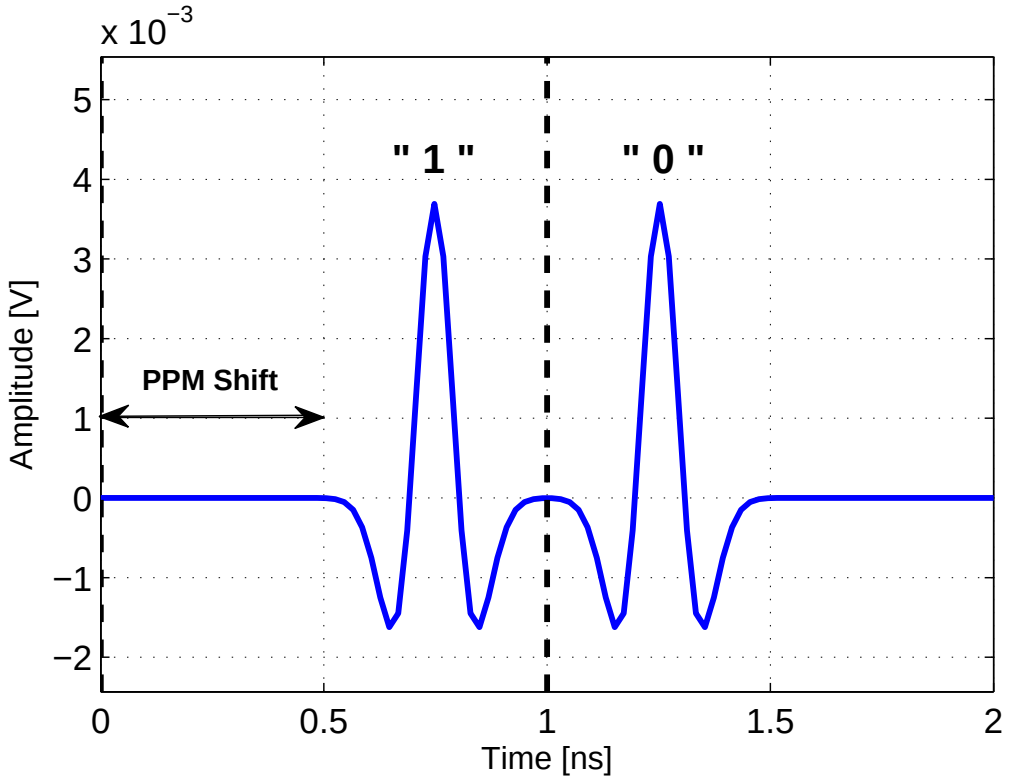

Figure 1.6: PPM modulation.

$$s_{PPM} = \sum_{q=0}^{Q-1} p(t - qT - a_q\epsilon) \tag{1.6}$$

where ϵ and a_q are the PPM shift and data symbol given by

$$a_q = \begin{cases} 0 & \text{represents bit "0"} \\ 1 & \text{represents bit "1"} \end{cases}.$$

PPM has a lower complexity and performance in compare with PAM modulation. A trade-off between complexity and performance can be achieved by using a combination of PAM and PPM, called pulse position amplitude modulation (PPAM) [12].

1.7 UWB Applications

UWB can be used in numerous applications. These applications can be categorized in two main groups, high data rate and low data rate. Typically, the closer the transmitter and the receiver are, the higher the achievable data rate. Both high data rate short range and low data rate long range communication systems are widely employed in industry. Some of the main applications are high data rate wireless local area network (WLAN), wireless personal area network (WPAN), wireless universal serial bus (WUSB), radio frequency identification (RFID), and home entertainment systems. Wall through imaging, vehicular applications, medical monitoring, rescue localization, and object positioning are some of lower date rate UWB applications [3].

Some of the potential applications for 60 GHz mm-wave communications are mobile broadband, high speed fixed wireless access, high speed WLANs, coaxial cable replacement for fast WPANs, wireless high definition multimedia interface (WHDMI) such as high definition television (HDTV), wireless digital video disc (DVD) player and cable box communications [7]. Application which required higher capacity such as coaxial cable replacement need at least 2Gb/s of data rate. Such capacity is achievable using 60 GHz mm-wave communications [13].

1.8 Thesis Summary and Outline

In this thesis, UWB is studied, concepts and history are discussed, and the advantages of UWB over narrow band are described. It is shown that UWB can provide a better data rate while having a lower probability of interference. Advantages and disadvantages of higher frequency UWB communications, 60 GHz mm-wave, in compare with the lower frequency UWB are discussed.

Different pulse modulations for UWB system have introduced. It is discussed why PPM is considered in this thesis as the chosen modulation technique. The rest of this thesis is organized as follow. In Chapter 2, time hopping (TH) technique is introduced. It is employed to the PPM modulation, TH-PPM, to reduce the interference in multiple access environments. Orthogonality and non-orthogonality of pulses are then discussed and compared. More over, TH-PPM is defined over additive white Gaussian noise (AWGN), Saleh-Valenzuela (SV) and Triple-SV (TSV) channel models. Each of these models discussed separately in details. In Chapter 3, different

types of rake receivers are introduced and compared. It is shown that ideal rake (I-Rake) receiver has the best performance among all rake receivers, followed by 5 finger selective rake (5S-Rake), 5 finger partial rake (5P-Rake), 2 finger selective rake (2S-Rake), and 2 finger partial rake (2P-Rake). High gain directional antennas are then introduced for 60 GHz mm-wave UWB. In Chapter 4, the bit error rate (BER) performance of TH-PPM over AWGN, SV and TSV channels is evaluated. Moreover, the performance of orthogonal and non-orthogonal TH-PPM with different numbers of users are compared. Performance results show that non-orthogonal TH-PPM can perform better than orthogonal TH-PPM when the number of users is large. It is shown that orthogonal and non-orthogonal TH-PPM modulation in a TSV channel performs close to TH-PPM modulation in a SV channel. Finally Chapter 5 concludes the thesis.

Chapter 2

UWB System Model

2.1 TH-PPM UWB Model

TH-PPM modulation uses the position of the pulses to modulate the binary data sequence. Time hopping is applied to this modulation for multi access environments. Time hopping code is a pseudo-random (PN) code that is unique for each user. In TH-PPM, the time frame is divided into several smaller time slots called chips. Each data bit is presented by one or more pulses where then each pulse, using TH code, is located randomly in a specific chip.

To transmit data in this system, the bit stream is first repetition encoded to obtain N_s pulses per bit. Time hopping is then applied to the output of the encoder, b_i, giving

$$C_i T_c + \epsilon b_{\lfloor i/N_s \rfloor}$$

where C_i, T_c and ϵ are the random code, chip duration, and PPM shift (applied to the pulse to differentiate between bits 0 and 1), respectively. We assume that $\epsilon < T_c$, $\epsilon \geq T_p$, and $C_i T_c + \epsilon < T_f$ where T_p and T_f are the pulse duration and frame time. The output of TH encoder is then modulated using PPM modulator which is given by

$$iT_f + C_i T_c + \epsilon b_{\lfloor i/N_s \rfloor}.$$

At this stage the position of unit pulses are set and ready to enter the pulse shaper filter to generate the pulse shaped TH-PPM signal. In Figure 2.1 the block diagram for TH-PPM is shown. The pulse shape of the TH-PPM signal must satisfy the FCC's spectral mask requirements. Sine, Gaussian (first and second derivative), and rectan-

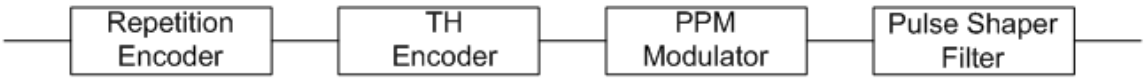

Figure 2.1: TH-PPM transmitter block diagram for UWB system

gular pulse shapes have been employed for this purpose [14]. The second derivative of the Gaussian pulse is used here since it satisfies the FCC spectral mask requirements and has been widely employed in UWB system designs [15]. The transmitted signal is then given by

$$s(t) = \sqrt{W} \sum_i p(t - iT_f - C_i T_c - \epsilon b_{\lfloor i/N_s \rfloor}) \tag{2.1}$$

where $\sqrt{W}$ is the signal amplitude. Fig. 2.2 illustrates a typical TH-PPM signal with $T_f = 3$ nsec, $T_c = 1$ nsec, $T_p = 0.5$ nsec, and a PPM shift of $\epsilon = 0.5$ nsec. The

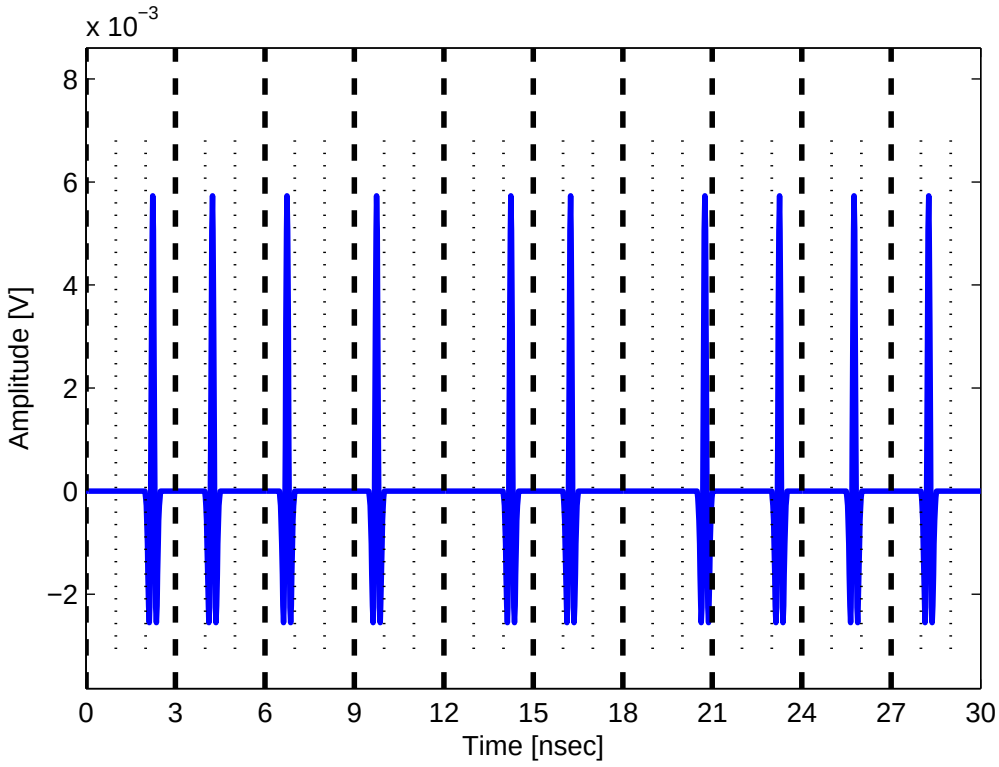

Figure 2.2: A TH-PPM signal with frame time $T_f = 3$ nsec, chip time $T_c = 1$ nsec, pulse duration $T_p = 0.5$ nsec, and PPM shift $\epsilon = 0.5$ nsec.

Gaussian pulse can be expressed as [16]

$$p(t) = \pm \frac{\sqrt{2}}{\alpha} e^{\frac{-2\pi t^2}{\alpha^2}} \tag{2.2}$$

where α^2 is the pulse shape factor equal to $4\pi\sigma^2$ (with variance σ^2). Hence, the second derivative is

$$p_2(t) = \left[1 - 4\pi \frac{t^2}{\alpha^2}\right] e^{-\frac{2\pi t^2}{\alpha^2}}. \tag{2.3}$$

Fig. 2.3 shows a typical second derivative Gaussian pulse waveform.

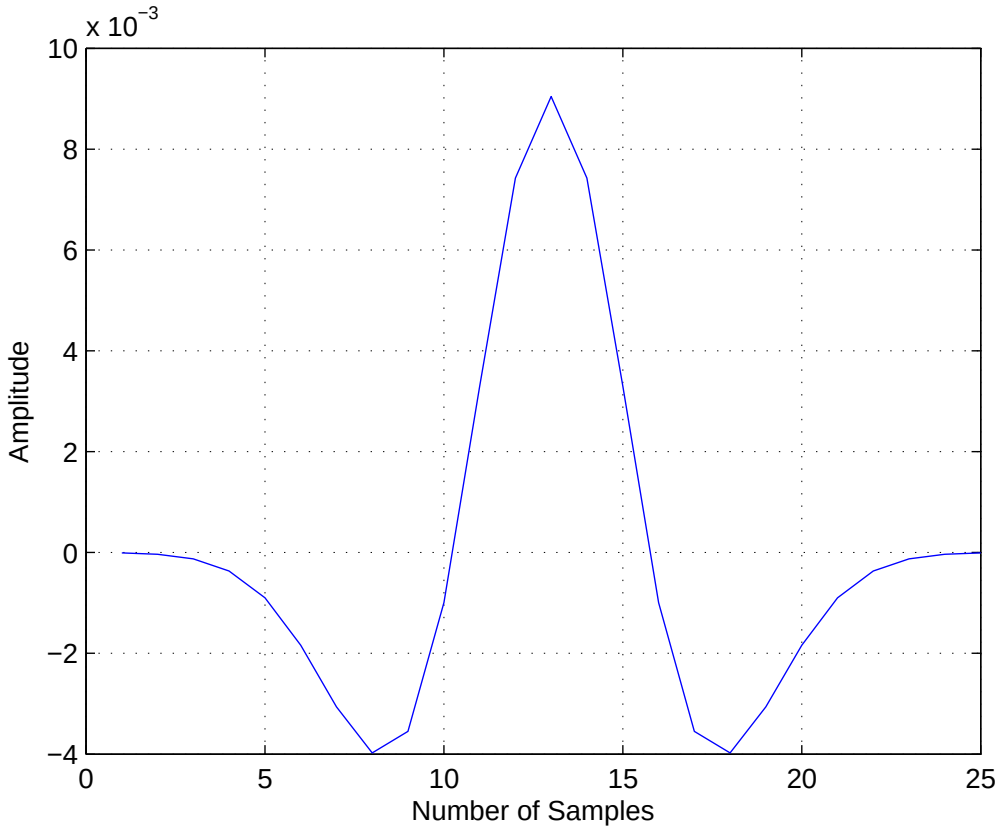

Figure 2.3: A typical second derivative Gaussian pulse waveform

For TH-PPM the pulse $p(t)$ is assumed to has non-zero values only in the interval of $[0, Tp]$. The transmitted signal is a series of pulses given by [17]

$$p_m(t) = \begin{cases} p(t + m\epsilon) & m\epsilon \leq t \leq m\epsilon + T_p \\ 0 & m\epsilon > t > m\epsilon + T_p \end{cases} \tag{2.4}$$

where $\epsilon < Tp$ for non-orthogonal TH-PPM, $\epsilon \geq Tp$ for orthogonal TH-PPM, and m is an integer.

2.2 UWB Channel Models

A channel can be modelled by calculating the physical processes that affect the transmitted signal. As the transmitted signal goes through the channel, it gets distorted

by multipath fading and Gaussian noise. Because transmission can be in a multiuser environment, the effect of multiuser interference must also be considered.The received signal is given by

$$r(t) = s(t) * h(t) + I(t) + n(t) \tag{2.5}$$

where $h(t)$ is the channel impulse response (CIR) which is convolved with the transmitted signal $s(t)$, and $I(t)$ and $n(t)$ are the interference from other users and additive white Gaussian noise, respectively.

The impulse response of the channel is

$$h(t) = \alpha\delta(t - \tau) \tag{2.6}$$

where $\delta()$, α and τ are the Dirac delta function, channel gain and delay, respectively. Using (2.5) and (2.6), the received signal is

$$r(t) = \alpha s(t - \tau) + I(t) + n(t). \tag{2.7}$$

The transmitted signal using TH-PPM modulation (2.1) can be expressed as

$$s(t) = \sqrt{W_{TX}} \sum_i p(t - iT_f - C_iT_c - \epsilon b_{\lfloor i/N_s \rfloor}) \tag{2.8}$$

where $\sqrt{W_{TX}}$ is the transmitted signal amplitude. From (2.7) and (2.8), the received signal is then

$$r(t) = \sqrt{W_{RX}} \sum_i p(t - iT_f - C_iT_c - \epsilon b_{\lfloor i/N_s \rfloor} - \tau) + I(t) + n(t) \tag{2.9}$$

where the received signal amplitude is given by, $\sqrt{W_{RX}} = \alpha\sqrt{W_{TX}}$.
$I(t)$ represents the interference from other users and is given by

$$I(t) = \sum_{u=1}^{U-1} \sqrt{W^{(u)}} \sum_i p(t - iT_f - C_i^{(u)}T_c - \epsilon b^{(u)}_{\left\lfloor i/N_s^{(u)} \right\rfloor} - \tau^{(u)}) \tag{2.10}$$

where $\sqrt{W^{(u)}}$ is the amplitude of the uth user signal. The received signal using (2.9)

and (2.10) is then

$$r(t) = \sqrt{W_{RX}} \sum_i p(t - iT_f - C_i T_c - \epsilon b_{\lfloor i/N_s \rfloor} - \tau) + \sum_{u=1}^{U-1} \sqrt{W^{(u)}} \sum_i p(t - iT_f - C_i^{(u)} T_c - \epsilon b^{(u)}_{\left\lfloor i/N_s^{(u)} \right\rfloor} - \tau^{(u)}) + n(t) \quad (2.11)$$

2.2.1 The Saleh-Valenzuela Model

The Saleh-Valenzuela (SV) model [18] is an UWB channel model which assumes the multipath components (rays) arrive at the receiver in groups called clusters [19]. The rays are delayed and attenuated replicas of the transmitted signal, and each cluster consists of several rays. Each cluster and each ray within a cluster has independent fading. The average power for the clusters and rays decays gradually. Both decay factors follow a Poisson distribution. This is illustrated in Fig. 2.4, which shows the instantaneous powers for the clusters and rays. Typically, the later the rays and clusters arrive, the lower the power of the rays and clusters. In this figure there are 14 clusters, and each contains 140 rays, which makes a total of 1960 rays.

Figs. 2.5 and 2.6 show the instantaneous and average power per cluster, respectively, with respect to the line of sight (LOS) signal component. In this case there are 14 clusters, and they arrive sequentially in time (i.e. cluster 8 arrives after cluster 7). It can be seen that in general the path loss increases as the delay increases. As a result the later clusters have less power compare to earlier ones (i.e. cluster 8 has less power than cluster 7).

Figure 2.7 [18] shows the SV channel model, where the cluster and ray arrival rates are Λ and λ, respectively. Γ and γ represent the cluster and ray power decay factors. Both clusters and rays arrive according to the Poisson distribution, but with different rates. Thus, the distributions of cluster and ray arrival times are

$$\begin{aligned} P(T_n|T_{n-1}) &= \Lambda e^{-\Lambda(T_n - T_{n-1})}, & n > 0 \\ P(\tau_n|\tau_{n,(m-1)}) &= \lambda e^{-\lambda(\tau_n - \tau_{n,(m-1)})}, & m > 0 \end{aligned} \quad (2.12)$$

where n is the cluster number and m is the ray number in the n-th cluster. T_n is the arrival time of the first ray in the n-th cluster, and $\tau_{n,(m-1)}$ is the delay of the $(m-1)$-th ray in the n-th cluster.

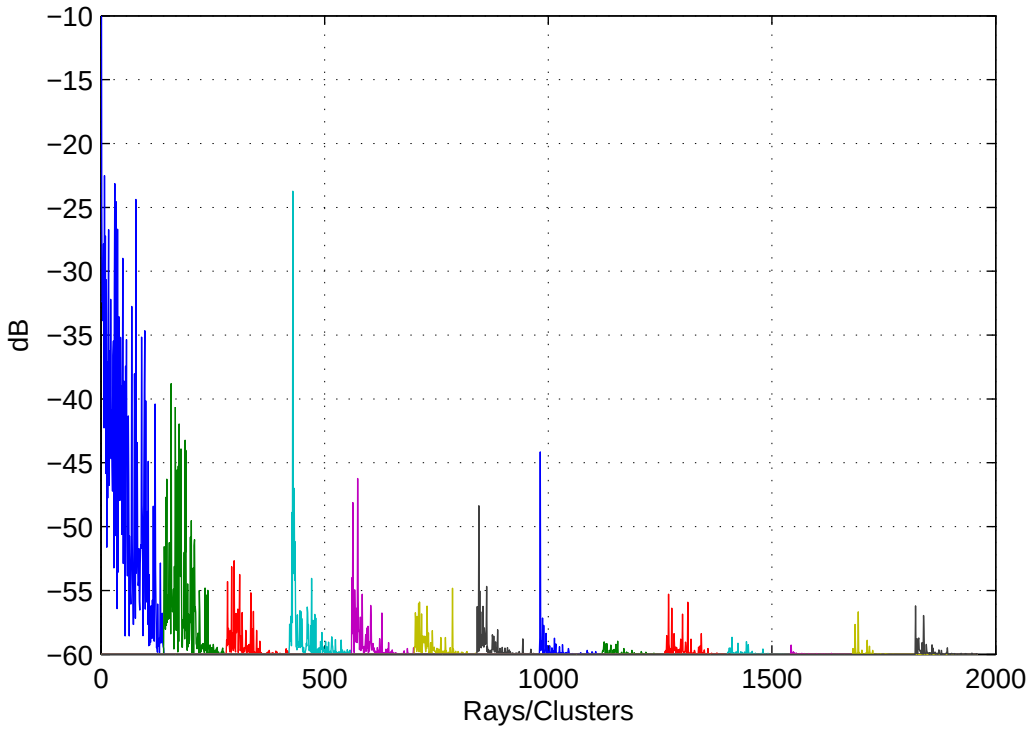

Figure 2.4: Ray and cluster instantaneous power for a typical SV channel.

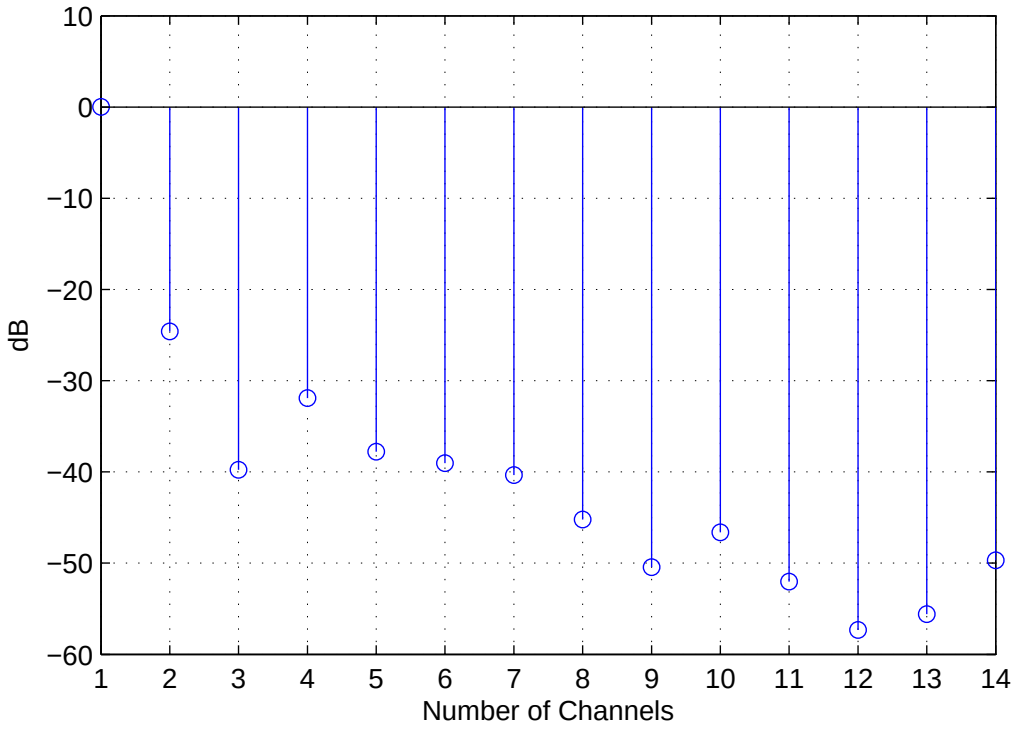

Figure 2.5: Instantaneous power per cluster for a typical SV channel.

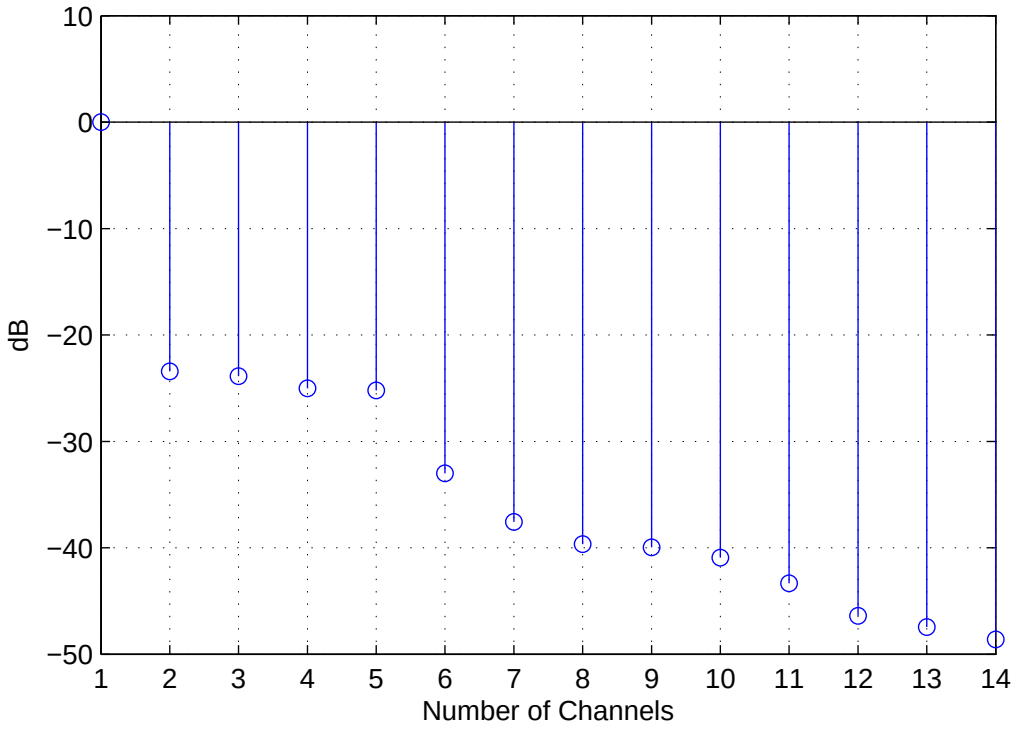

Figure 2.6: Average power per cluster for a typical SV channel.

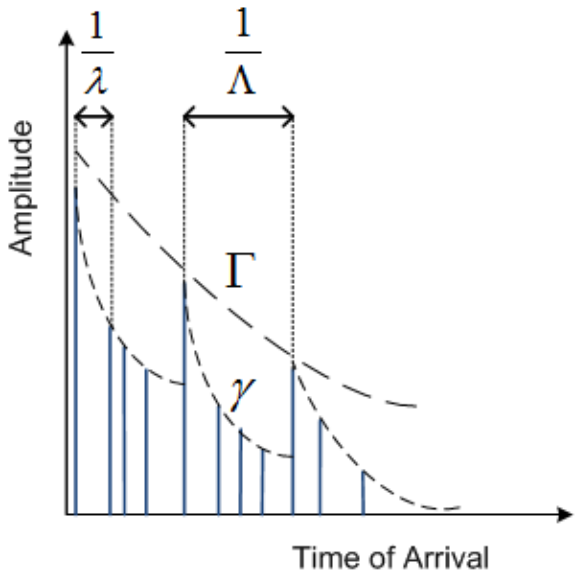

Figure 2.7: The SV channel impulse response with ray arrival rate λ, cluster arrival rate Λ, ray power decay factor γ, and cluster power decay factor Γ.

The channel impulse response for this model is

$$h(t) = A \sum_{n=1}^{N} \sum_{m=1}^{M} \alpha_{nm} \delta(t - T_n - \tau_{nm}) \tag{2.13}$$

where A is the path loss due to shadowing and is modeled as a log-normal random variable. M and N are the number of rays and clusters, respectively. α_{nm} is the multipath gain coefficient of the m-th ray in the n-th cluster defined as

$$\alpha_{nm} = P_{nm} \beta_{nm} \tag{2.14}$$

where P_{nm} is a uniform random variable with value from ± 1 which defines the random pulse inversion that happens because of reflections. β_{nm} is the lognormal fading term which can be modelled as

$$\beta_{nm} = 10^{\chi_{nm}/20} \tag{2.15}$$

$$\chi_{nm} = \mu_{nm} + \zeta_n + \zeta_{nm} \tag{2.16}$$

where ζ_n and ζ_{nm} are zero-mean Gaussian random variables with variances σ_ξ^2 and σ_ζ^2, respectively. They define the channel gain fluctuations for the clusters and rays.

$$\mu_{nm} = K - \frac{T_n}{\Gamma} - \frac{\tau_{nm}}{\gamma} \tag{2.17}$$

where K is a constant, and Γ and γ are the cluster and ray power decays. Using (2.5), (2.8) and (2.13) the received signal is

$$r(t) = \sqrt{W_{RX}} \sum_{i} \sum_{n=1}^{N} \sum_{m=1}^{M} \alpha_{nm} p(t - iT_f - C_i T_c - \epsilon b_{\lfloor i/N_s \rfloor} - T_n - \tau_{nm}) \tag{2.18}$$
$$+ \sum_{u=1}^{U-1} \sqrt{W^{(u)}} \sum_{i} \sum_{n=1}^{N} \sum_{m=1}^{M} \alpha_{nm} p(t - iT_f - C_i^{(u)} T_c - \epsilon b^{(u)}_{\left\lfloor i/N_s^{(u)} \right\rfloor} - T_n - \tau^{(u)}) + n(t)$$

where $\sqrt{W_{RX}} = A\sqrt{W_{TX}}$.

The power delay profile (PDP) of the UWB channel (using IEEE 802.15.3a-CM1 channel parameters) is shown in Fig. 2.8. The PDP is a graphical view of signal intensity as a function of time delay with respect to the arrival of the first signal, which is assumed to have zero delay. It is calculated as the expected value of the

magnitude squared channel impulse response, and is given by [20]

$$PDP = E[|h(\tau)|^2]. \tag{2.19}$$

Fig. 2.9 shows the PDP of the UWB channel using IEEE 802.15.3a-CM4 parameters.

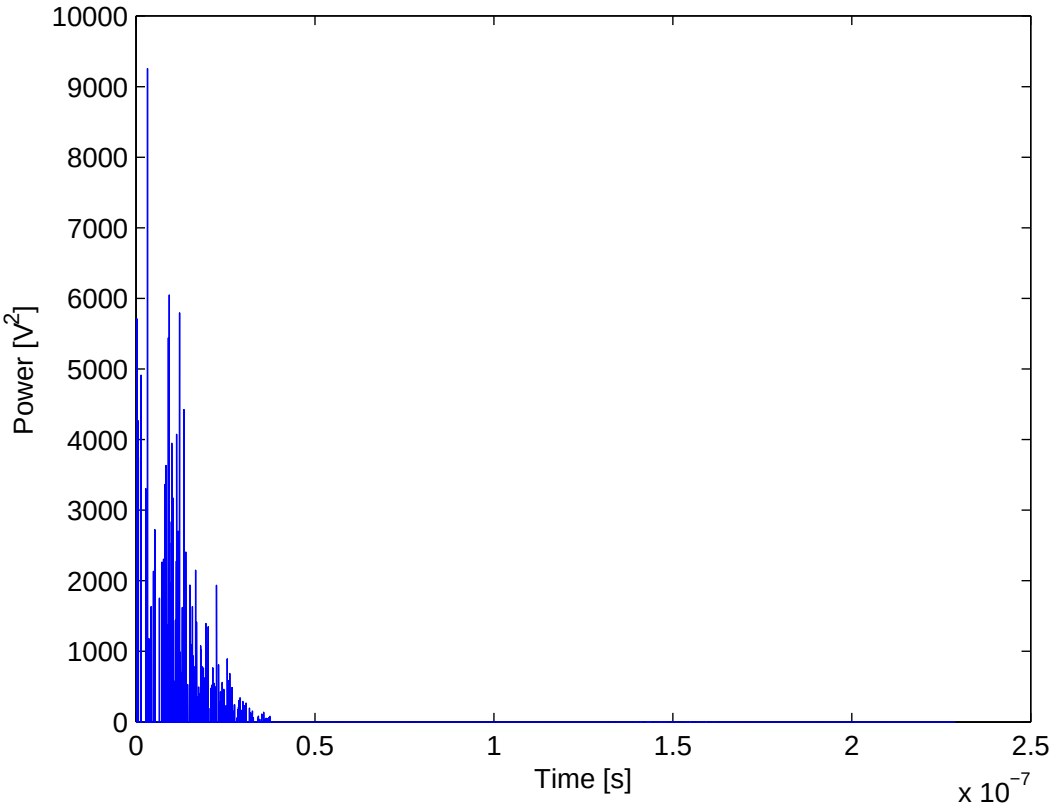

Figure 2.8: Power delay profile for UWB channel model CM1.

More arrivals occur at the receiver for channel CM4, as the fading is the more severe in non-line-of-sight (NLOS). Due to the longer duration of the CM4 channel impulse response, the time separation between pulses must be carefully chosen to avoid inter-symbol interference (ISI).

A discrete time channel impulse response is employed for multipath environments so that performance can be practically evaluated. In this model, the time dimension is divided into small time intervals called bins. Each bin can contain one or more multipath components. Figs. 2.10 and 2.11 show the corresponding discrete time impulse responses for channels CM1 and CM4. Since CM4 represents an extreme

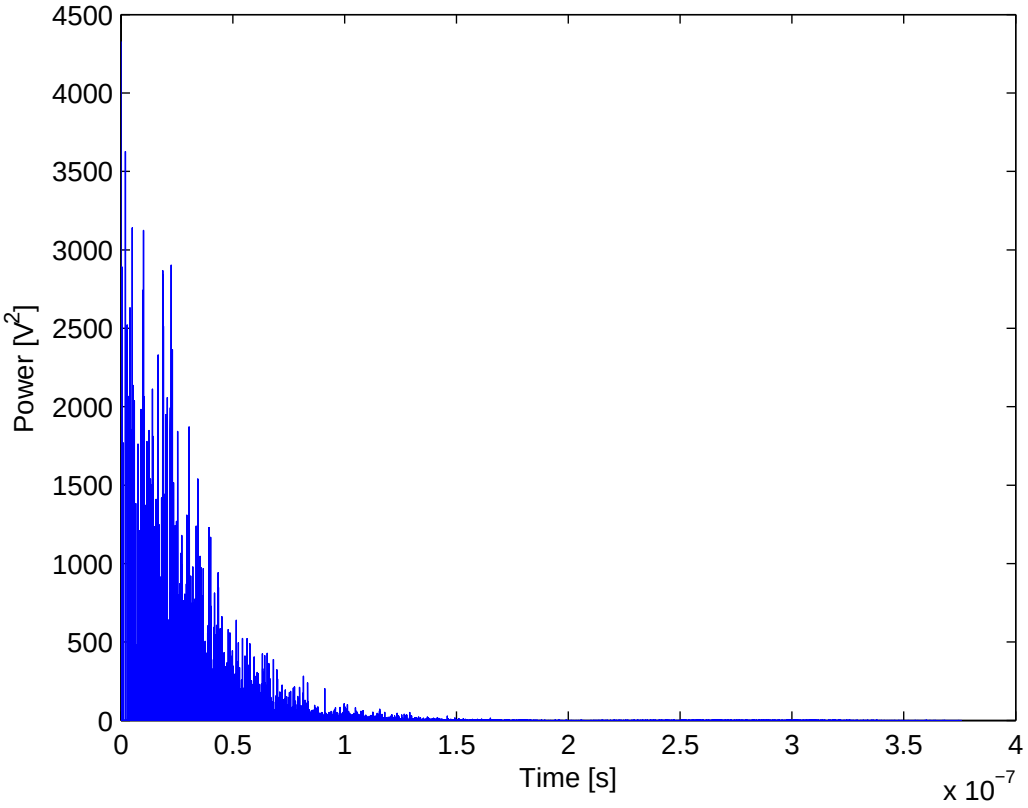

Figure 2.9: Power delay profile for UWB channel model CM4.

NLOS channel, the discrete CIR has more multipath components compare to channel CM1.

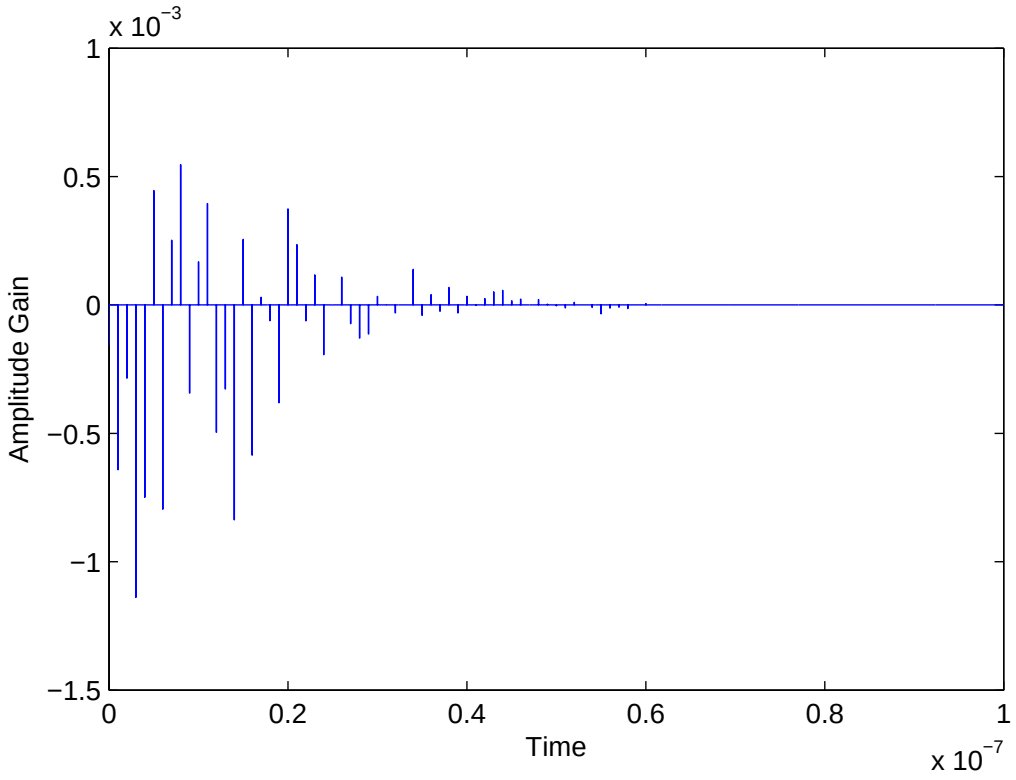

Figure 2.10: Discrete time impulse response for UWB channel model CM1.

2.2.2 The Triple S-V Model

The triple-SV (TSV) model [21] is a combination of the SV model [18] and the two path model [22]. It was developed and found by Shoji, Sawada, Saleh and Valenzuela. This channel model is considered appropriate for the 60 GHz mm-wave UWB channel.

The SV model discussed previously does not consider the angle of arrival (AoA). However, antenna directivity has a significant impact on the signal to noise ratio for high frequencies such as with mm-wave signals. Hence the TSV channel model considers the AoA. In this case, the channel impulse response for the SV channel model is defined as

$$h(t) = \sum_{n=1}^{N} \sum_{m=1}^{M} \alpha_{nm} \delta(t - T_n - \tau_{nm}) \delta(\phi - \Psi_n - \psi_{nm}) \tag{2.20}$$

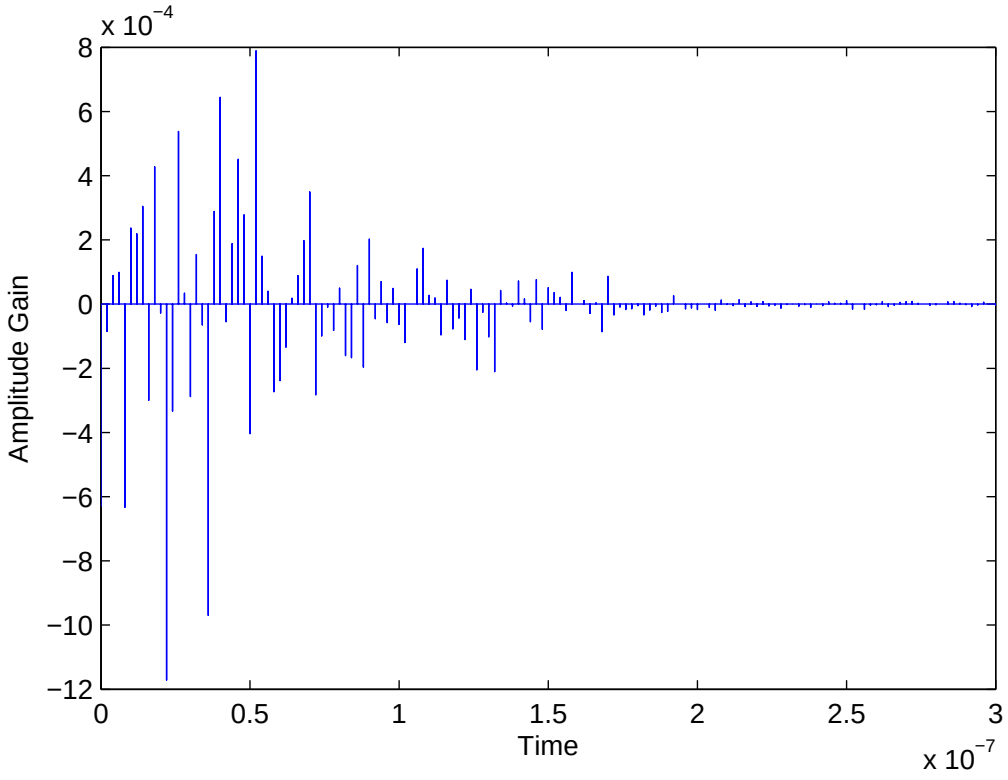

Figure 2.11: Discrete time impulse response for UWB channel model CM4.

where Ψ_n is the AoA of the n-th cluster and ψ_{nm} is the AoA of the m-th ray. ψ_{nm} is assumed to have a Laplacian distribution

$$p(\psi_{nm}) = \frac{1}{\sqrt{2}\sigma_\phi} e^{-\sqrt{2}\psi_{nm}/\sigma_\phi}. \tag{2.21}$$

σ_ϕ is the angle spread of the rays, and α_{nm} is the m-th ray n-th cluster gain and can be presented as

$$\overline{|\alpha_{nm}|^2} = \Omega_0 e^{\frac{-T_n}{\Gamma}} e^{\frac{-\tau_{nm}}{\gamma}} \sqrt{G_r(0, \Psi_n + \psi_{nm})} \tag{2.22}$$

where G_r is the receiver antenna gain, and $\angle\alpha_{nm}$ is a uniform random variable distributed over $[0, 2\pi)$. The parameters $\Gamma, \Lambda, \gamma, \lambda, \sigma_1(\sigma_\zeta), \sigma_2(\sigma_\xi)$ are the same as in

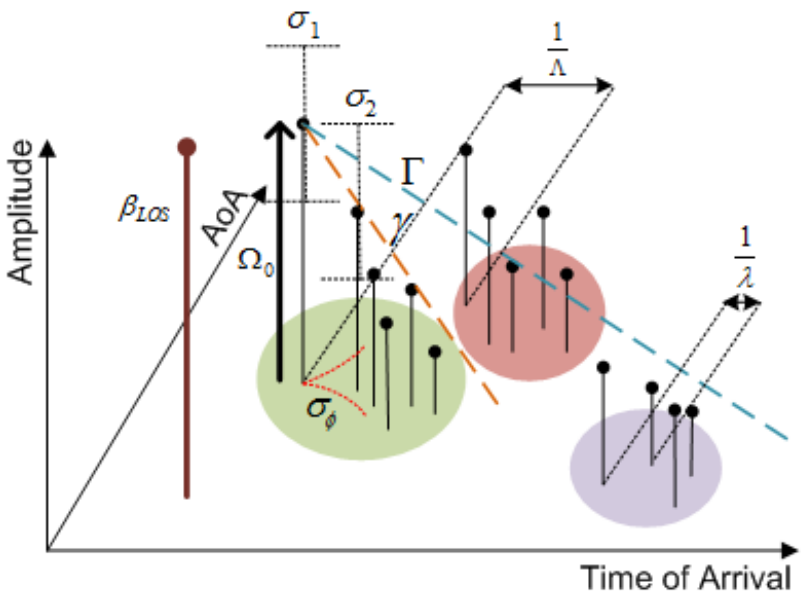

Figure 2.12: A typical TSV channel model realization.

Section 3.1. The remaining parameters are σ_ϕ and Ω_0, which are the angle spread of the rays with Laplace distribution, and the average power of the first ray of the first cluster, respectively. Fig. 2.12 [23] represents a typical TSV channel model realization where β_{LOS} is the line of sight (LOS) component.

The second component of the TSV model is based on a two-path model and is given by

$$\beta = \frac{\mu_D}{D} \left| G_{t1}G_{r1} + G_{t2}G_{r2}\Gamma_0 exp\left[j\frac{2\pi}{\lambda_f}\frac{2h_1h_2}{D} \right] \right| \tag{2.23}$$

where D is the distance between the transmit and receive antennas, and h_1, h_2 are the

antenna heights. λ_f, Γ_0, and μ_D are the wavelength of center frequency, the reflection coefficient, and the average distance distribution. G_{t1} and G_{r1} are the transmitter and receiver gains for the direct path d_1, and G_{t2} and G_{r2} are the transmitter and receiver gains for the reflected path d_2. The value of β is very sensitive to small antenna movements, even on order of a few millimeters. The two path model is illustrated in Fig. 2.13 [22].

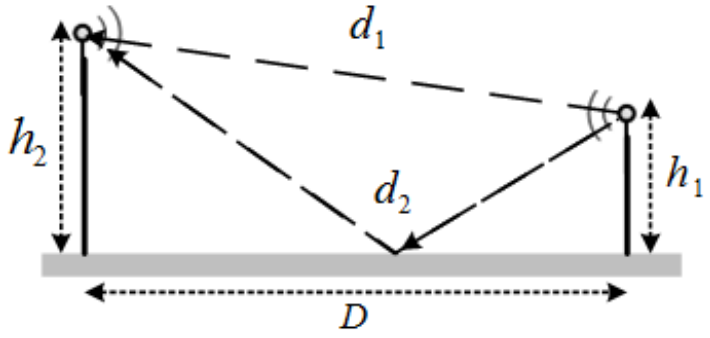

Figure 2.13: The two path channel model.

Combining (2.20) and (2.23), the TSV channel model is

$$h(t) = \beta\delta(t) + \sum_{n=1}^{N}\sum_{m=1}^{M} \alpha_{nm}\delta(t - T_n - \tau_{nm})\delta(\phi - \Psi_n - \psi_{nm}) \tag{2.24}$$

where $\beta\delta(t)$ represents the LOS component and the remaining terms represent the SV model component.

The average power of the channel can be represented as a function of the angle of arrival, which is called the power azimuth profile. Based on the power azimuth profile, the distribution of the cluster mean AoA can be described by a uniform distribution over $[0, 2\pi]$, i.e.,

$$p(\Theta_n|\Theta_{n-1}) = \frac{1}{2\pi}, \quad (n > 0). \tag{2.25}$$

Fig. 2.14 shows a 3D realization of the clusters with respect to power, angle of arrival and time of arrival. It can be seen that the later the clusters and rays arrive, the lower the power is. This figure also shows that the clusters arrive with different angles.

The main TSV channel model parameters which determine the performance are power decay profile (PDP), mean excess delay and root mean square (RMS) delay

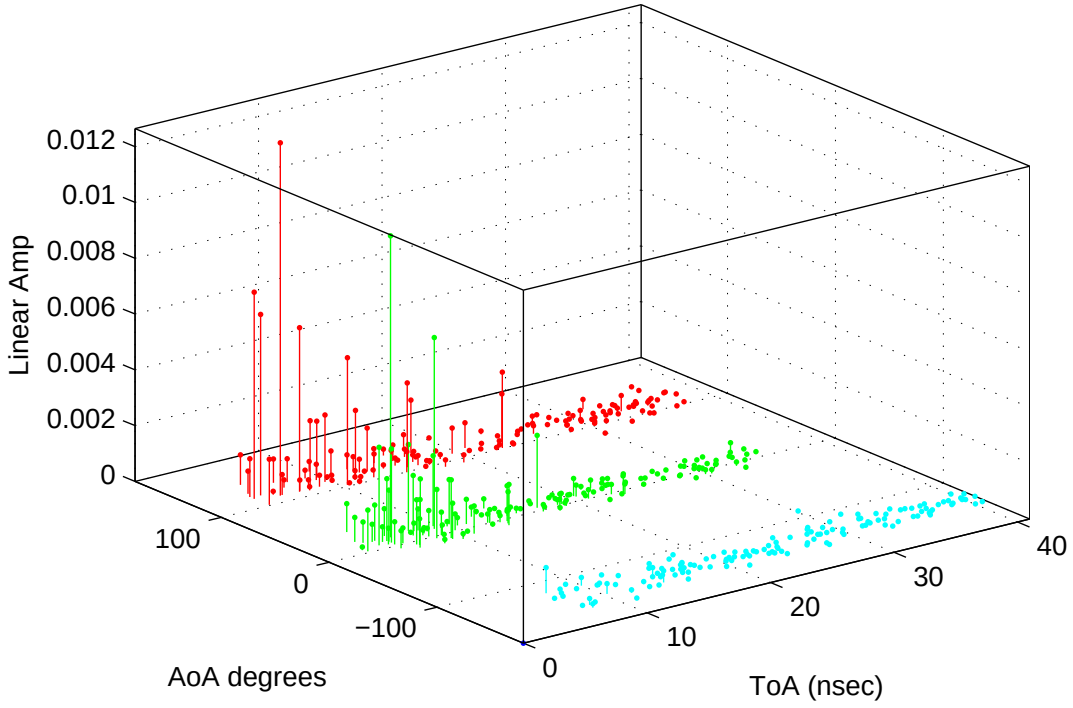

Figure 2.14: A 3D realization of a typical TSV channel impulse response with respect to ToA, AoA and amplitude.

spread. A typical PDP for the TSV channel is shown in Fig. 2.15. The LOS component is located at the zero position with power of -81.9842 dB. The average PDP for this channel model is shown in Fig. 2.16.

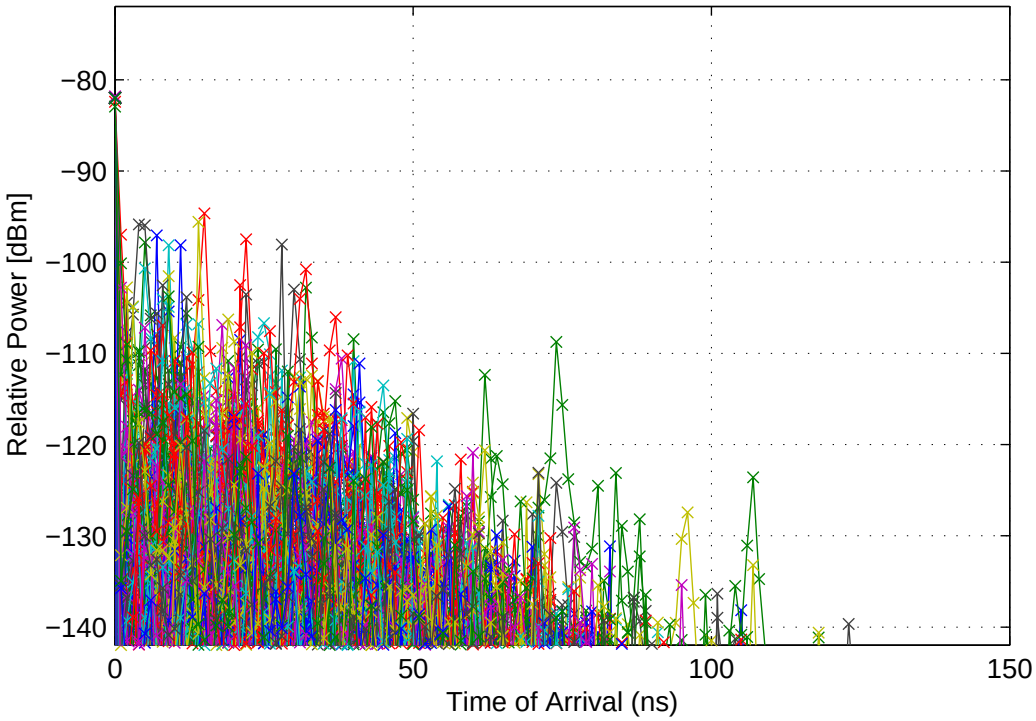

Figure 2.15: A typical power delay profile for the TSV channel.

The mean excess delay is the weighted average or the first moment of the power delay profile, and is given by [20]

$$\overline{\tau} = \frac{\sum_k a_k^2 \tau_k}{\sum_k a_k^2} = \frac{\sum_k P(\tau_k)\tau_k}{\sum_k P(\tau_k)}. \tag{2.26}$$

In Figure 2.17 the mean excess delay of TSV channel is illustrated. For this figure, the standard deviation of the log normal variable for cluster fading is 6.6300 nsec.

The RMS delay spread is the square root of the second central moment of the PDP and is given by [20]

$$\sigma_\tau = \sqrt{\overline{\tau^2} - (\overline{\tau})^2} \tag{2.27}$$

where

$$\overline{\tau^2} = \frac{\sum_k a_k^2 \tau_k^2}{\sum_k a_k^2} = \frac{\sum_k P(\tau_k)\tau_k^2}{\sum_k P(\tau_k)}. \tag{2.28}$$

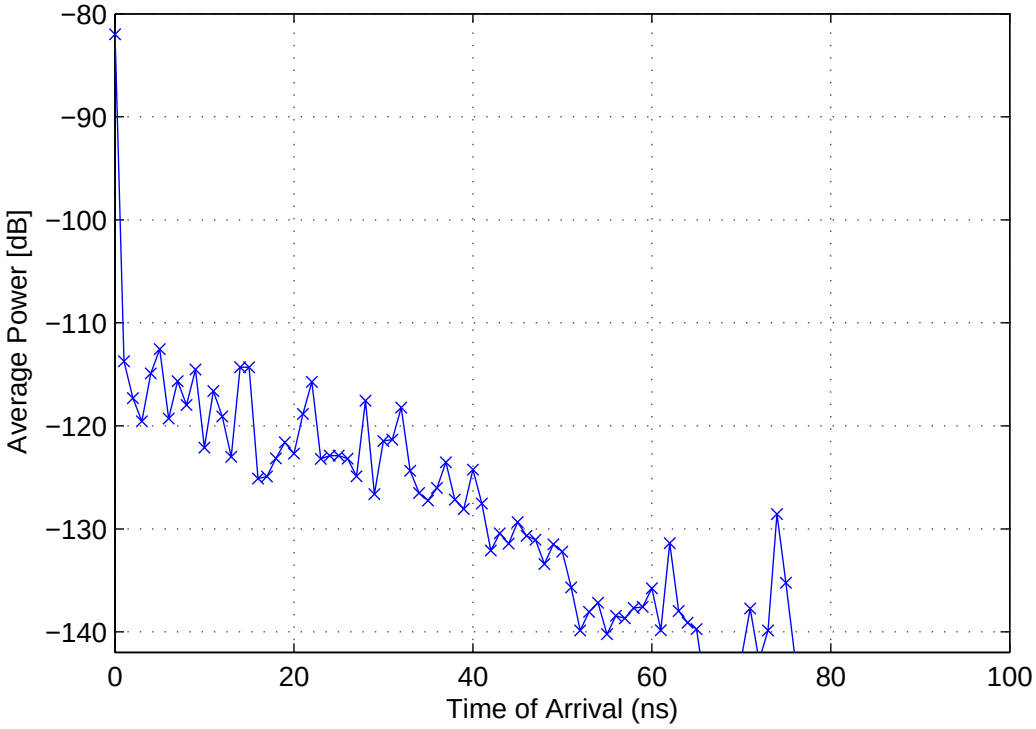

Figure 2.16: Average power delay profile for a typical TSV channel.

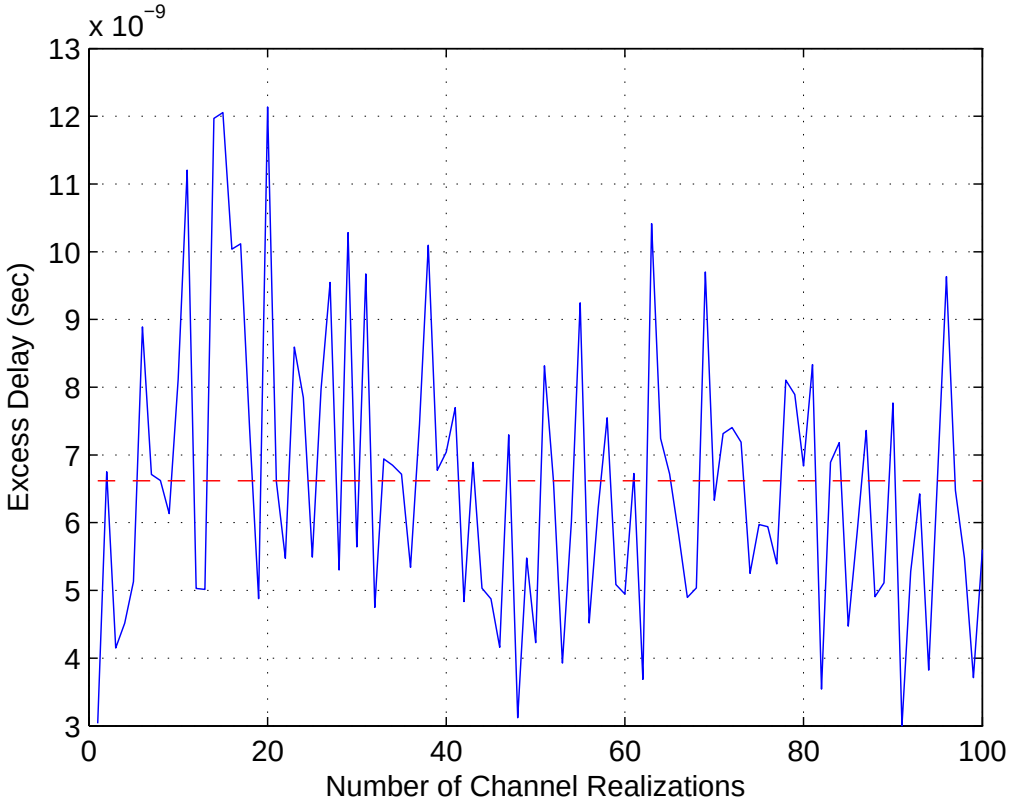

Figure 2.17: The channel excess delay.

The RMS delay spread is a measure of the effective duration of the channel and is shown in Figure 2.18. In this figure, the standard deviation of the log normal variable for ray fading is equal to 9.8300 nsec.

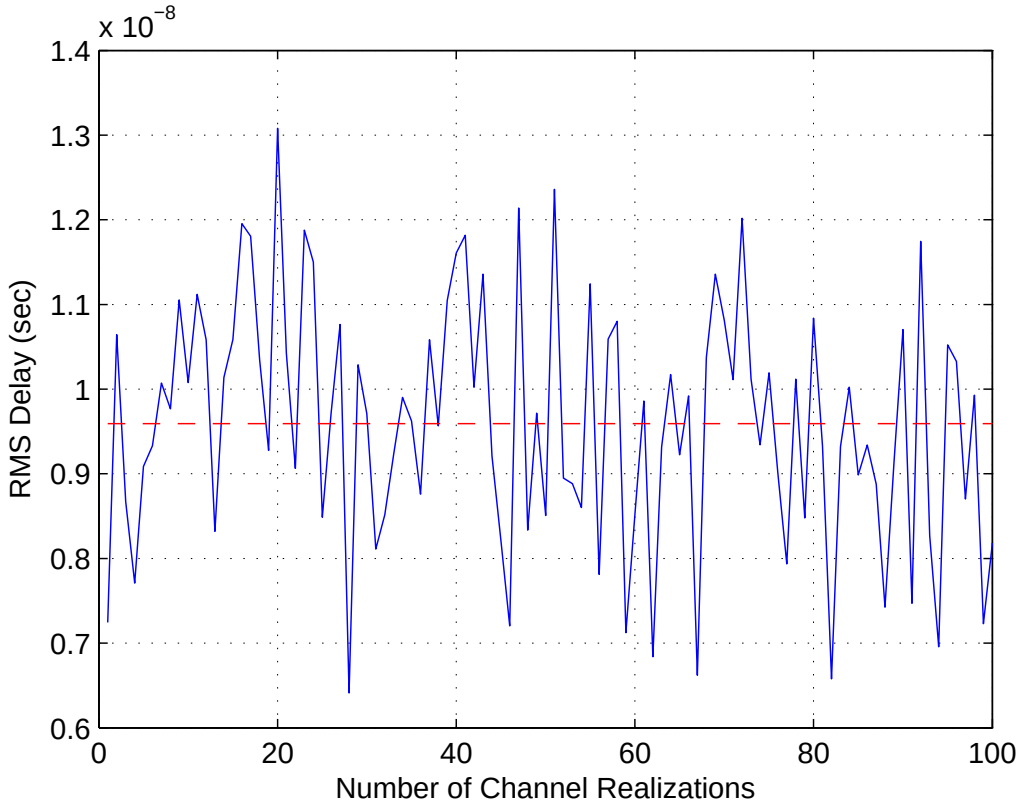

Figure 2.18: TSV Channel model RMS delay spread.

Since channel impulse response is random, in the simulation more than one realization is required to make the results more realistic. 100 realizations is used here in this thesis and in Figure 2.19 the continuous impulse response for these 100 realizations is shown. In Figure 2.20, the real and imaginary parts of the channel impulse response realizations are given.

2.3 Summary

In this chapter, TH-PPM model and a recommended pulse shape for UWB are introduced, and orthogonality and non-orthogonality of these pulses are discussed accordingly.

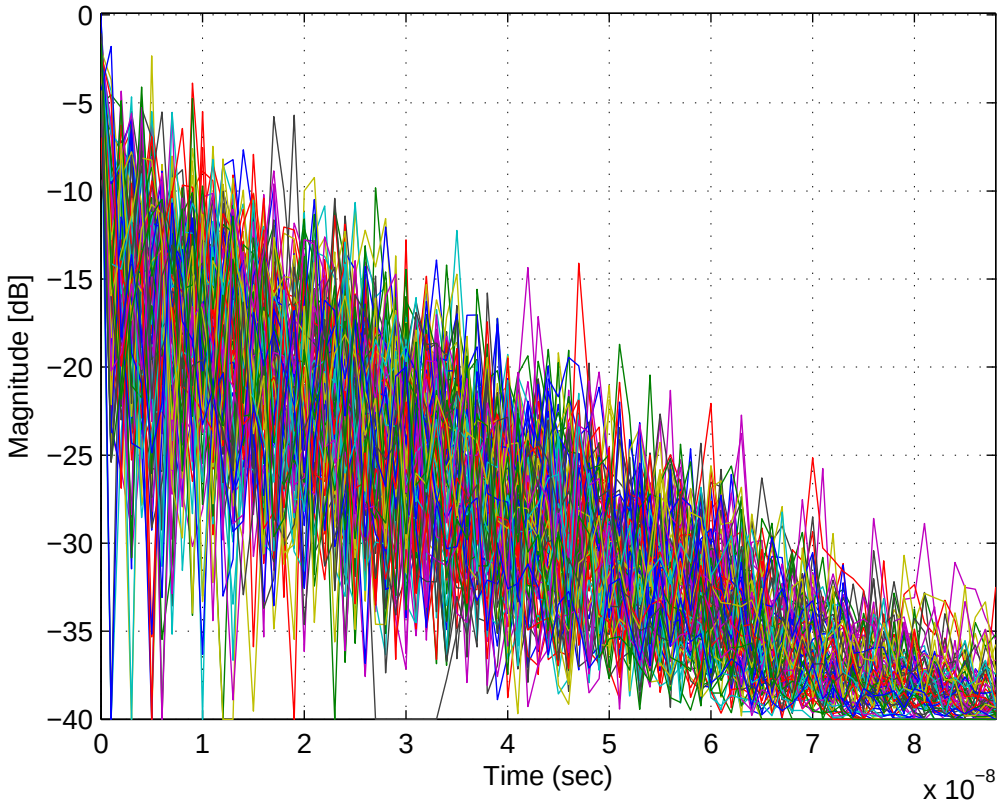

Figure 2.19: The continuous channel impulse response for 100 realizations of the mm-wave UWB channel.

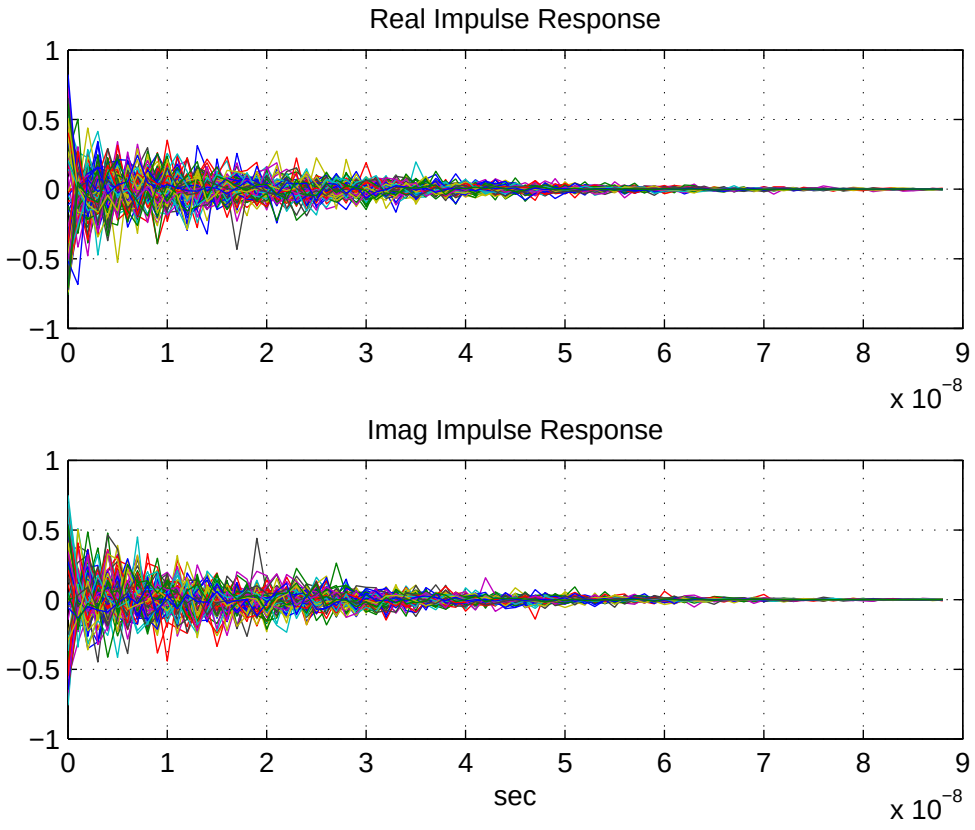

Figure 2.20: Image and real demonstaration of impulse response realization

In the channel model section, channel impulse response is defined and the transmitted and received signals are modeled. Two UWB channels namely SV and TSV are introduced for lower frequency UWB and 60 GHz mm-wave UWB communications. It is discussed in SV channel that the delayed and attenuated replicas of transmitted signal, rays, arrive in groups of clusters. It is shown that the average power of rays and clusters decays gradually which are following the Poisson distribution but with different rates. The impulse response and the power delay profile of two different scenarios of this model is shown and compared.

TSV channel model is considered for mm-wave UWB communications, which is a combination of SV and two-path channel models. In this model, angle of arrival is added to the SV channel since antenna directivity is an important factor in higher frequency communications such as mm-wave UWB. The main channel parameters such as power decay profile, mean excess, and root mean square delay are defined and shown in this chapter.

Chapter 3

UWB Receiver Model

3.1 Optimum Receiver

One of the main challenges in wireless communications is to design a receiver which can provide an accurate estimate of the transmitted signal with good performance in noise, fading, and interference. Good performance must be achieved with reasonable system complexity, such as with the optimum pulse detection receiver in [16].

From (2.7), the received signal in an AWGN fading channel is $r(t) = \alpha s(t-\tau) + I(t) + n(t)$. With M-ary TH-PPM, $s(t)$ consists of J different waveforms $s_j(t)$. Each of these waveforms can be generated by a basis function which is given by [24]

$$s_j(t) = \sum_{i=0}^{J-1} s_{ji} j_i(t). \tag{3.1}$$

As a result s_{ji} can be calculated as

$$s_{ji} = \int_0^T s_j(t) j_i(t) dt. \tag{3.2}$$

The basis functions for 2-ary TH-PPM are given by

$$j_i(t) = p_0(t - iT_f - C_i T_c - \epsilon b_{\lfloor i/N_s \rfloor}) \tag{3.3}$$

where $b_{\lfloor i/N_s \rfloor}$ can be either 0 or 1.

The received signal $r(t)$ goes through a correlator system which consist of J cross correlators, so the received signal is multiplied by $j_0(t-\tau)$ to $j_{J-1}(t-\tau)$. The

mathematical operation of cross correlator is to integrate the received signal with a replica of the transmitted signal over the interval of one symbol [6]. For 2-ary TH-PPM, to detect bits 0 and 1, the correlator consists of two cross correlators. One multiplies the received signal by $j_0(t-\tau)$, and the other by $j_1(t-\tau)$. Using (3.3), we have

$$\begin{cases} j_0(t-\tau) = p_0(t - iT_f - C_iT_c - \tau) \\ j_1(t-\tau) = p_0(t - iT_f - C_iT_c - \epsilon - \tau) \end{cases}. \tag{3.4}$$

However, for 2-ary TH-PPM, the receiver can be implemented with only one cross correlator, which results in lower complexity [24]. The single cross correlator is a combination of the two cross correlators in (3.4), using $j(t) = j_0(t) - j_1(t)$. Based on this, the basis function in the new cross corelator is given by

$$j(t-\tau) = p_0(t - iT_f - C_iT_c - \tau) - p_0(t - iT_f - C_iT_c - \epsilon - \tau). \tag{3.5}$$

The received signal (2.7) is multiplied by $j(t-\tau)$, and the result is input to the integrator. The output of the cross correlation function is the decision variable, Z.

$$Z = \int_{\tau}^{N_sT_f+\tau} r(t)j(t-\tau)dt. \tag{3.6}$$

The correlator is in charge of converting the received signal into a set of decision variables [24]. Using (2.7), (3.5) and (3.6) we have

$$Z = \int_{\tau}^{N_sT_f+\tau} [\alpha s(t-\tau)+I(t)+n(t)].[p_0(t-iT_f-C_iT_c-\tau)-p_0(t-iT_f-C_iT_c-\epsilon-\tau)]dt. \tag{3.7}$$

To simplify the calculations, the decision variable components are calculated separately.

$$Z = Z_{RX} + Z_I + Z_n \tag{3.8}$$

where Z_{RX}, Z_I and Z_n are decision variable for $\alpha s(t-\tau)$, interference and noise respectively, and can be calculated as

$$Z_{RX} = \int_{\tau}^{N_sT_f+\tau} s_{RX}(t).[p_0(t - iT_f - C_iT_c - \tau) - p_0(t - iT_f - C_iT_c - \epsilon - \tau)]dt \tag{3.9}$$

$$Z_I = \int_{\tau}^{N_sT_f+\tau} I(t).[p_0(t - iT_f - C_iT_c - \tau) - p_0(t - iT_f - C_iT_c - \epsilon - \tau)]dt \tag{3.10}$$

and

$$Z_n = \int_{\tau}^{N_s T_f + \tau} n(t).[p_0(t - iT_f - C_i T_c - \tau) - p_0(t - iT_f - C_i T_c - \epsilon - \tau)]dt. \quad (3.11)$$

Using (2.9) and (3.9) we get

$$Z_{RX} = \int_{\tau}^{N_s T_f + \tau} [\sqrt{W_{RX}} \sum_i p(t - iT_f - C_i T_c - \epsilon b_{\lfloor i/N_s \rfloor} - \tau)] \quad (3.12)$$
$$\cdot [p_0(t - iT_f - C_i T_c - \tau) - p_0(t - iT_f - C_i T_c - \epsilon - \tau)]dt$$

$$Z_{RX} = \sqrt{W_{RX}} \int_{\tau}^{N_s T_f + \tau} [\sum_i p(t - iT_f - C_i T_c - \epsilon b_{\lfloor i/N_s \rfloor} - \tau) \cdot p_0(t - iT_f - C_i T_c - \tau) \quad (3.13)$$
$$- \sum_i p(t - iT_f - C_i T_c - \epsilon b_{\lfloor i/N_s \rfloor} - \tau) \cdot p_0(t - iT_f - C_i T_c - \epsilon - \tau)]dt$$

$$Z_{RX} = N_s \sqrt{W_{RX}} \int_0^{T_f} [p(t - \epsilon b) \cdot p_0(t) - p(t - \epsilon b) \cdot p_0(t - \epsilon)]dt. \quad (3.14)$$

In the case that bit 0 is transmitted

$Z_{RX} = N_s \sqrt{W_{RX}} \int_0^{T_f} [p(t) \cdot p_0(t) - p(t) \cdot p_0(t - \epsilon)]dt$

$Z_{RX} = N_s \sqrt{W_{RX}}(1 - \rho(\epsilon))$

and for bit 1

$Z_{RX} = N_s \sqrt{W_{RX}} \int_0^{T_f} [p(t - \epsilon) \cdot p_0(t) - p(t - \epsilon) \cdot p_0(t - \epsilon)]dt$

$Z_{RX} = N_s \sqrt{W_{RX}}(\rho(\epsilon) - 1) = -N_s \sqrt{W_{RX}}(1 - \rho(\epsilon))$

where $\rho(\epsilon)$ is the auto-correlation function and is equal to

$$\rho(\epsilon) = \int_0^{T_f} [p_0(t) \cdot p_0(t - \epsilon)]dt. \quad (3.15)$$

Using (2.10), the decision variable for the interference, Z_I, is a zero mean random

variable equal to [24]
$\sigma_I^2 = \frac{N_s}{T_s}\sigma_X^2 \sum_{u=1}^{U} W^{(u)}$
where σ_X^2 is a constant and depends on both the pulse shape and the PPM shift [24]. Noise is a random variable with uniform double-sided power spectral density (PSD) of $\frac{N_0}{2}$. PSD characterizes the power distribution of a signal in frequency domain [6]. The noise decision variable Z_n, has zero mean and variance

$$\sigma_n^2 = N_s N_0 (1 - \rho(\epsilon)).$$

Variance determines the randomness of a random variable [6].

Based on the decision variable Z, the detector decides which waveform signal was transmitted. The output of the optimum detector using (3.8) and (3.14) is given by

$$Z = \begin{cases} N_s\sqrt{W_{RX}}(1-\rho(\epsilon)) + Z_I + Z_n & bit\text{“0”} \\ -N_s\sqrt{W_{RX}}(1-\rho(\epsilon)) + Z_I + Z_n & bit\text{“1”} \end{cases} \tag{3.16}$$

which shows that if $Z > 0$, the optimum detector esitmate is bit “0”, and if $Z < 0$, bit “1” is estimated. A block diagram of the optimum receiver is shown in Fig. 3.1.

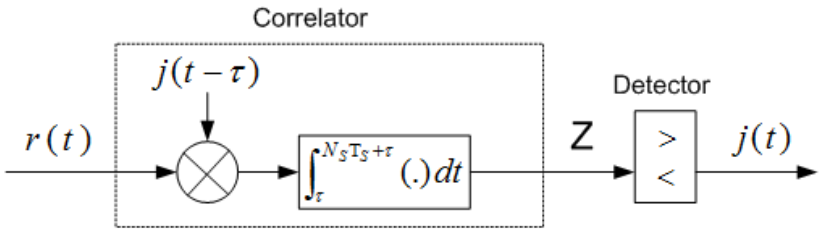

Figure 3.1: Optimum receiver block diagram.

The bit error probability of the system can be calculated as [6]

$$P_B = \frac{1}{2}P(Z|bit(0)) + \frac{1}{2}P(Z|bit(1))$$

where $P(Z|bit(0))$ and $P(Z|bit(1))$ are the probability density function (pdf) of likeli-

hood transfered values of "0" and "1". However, due to the equal a priori probabilities

$$P_B = P(Z|bit(0)) = P(N_s\sqrt{W_{RX}}(1-\rho(\epsilon)) + Z_i + Z_n < 0)$$

The average bit error probability is given by [24]

$$P_B = \frac{1}{2}\text{erfc}\left(\sqrt{\frac{1}{2}\left(\left(N_s\frac{W_{RX}}{N_0}\left(1-\rho(\epsilon)\right)\right)^{-1} + \left(\frac{\left(1-\rho(\epsilon)\right)^2}{R_b\sigma_X^2\sum_{u=1}^{U}\frac{W^{(U)}}{W_{RX}}}\right)^{-1}\right)^{-1}}\right) \quad (3.17)$$

where R_b denotes the user bit rate.

3.2 Rake Receiver

To obtain acceptable performance, the optimum receiver should employ additional correlators for use in the SV channel. These are used for the different replicas of the transmitted waveform. Such an approach is called a rake receiver [24]. Rake receivers combine the replicas which are chosen using several different fingers.

The correlators in the receiver are delayed appropriately to provide the best signal estimate. Space diversity or antenna diversity is used to provide diversity in the system by using multiple receiving antennas. Several space diversity reception methods exist which can be used with rake receivers. Maximum ratio combining (MRC) is a commonly used technique and is the one utilized here. MRC weights the branches according to their signal to noise power ratios and then sums them together [20]. A block diagram of a typical rake receiver is shown in Fig. 3.2 [20].

Three different types of rake receiver are considered here. The ideal rake (I-Rake) receiver detects all L_I multipath components of the same signal, so L_I is the number of fingers in the receiver. The I-Rake receiver is illustrated in Figure 3.3. The partial rake (P-Rake) receiver detects the first L_P components that arrive at the receiver. Figure 3.4 shows a P-Rake receiver with 5 fingers. A selective rake (S-Rake) receiver is shown in Figure 3.5. The name comes from the fact that in this method, receiver selects the L_S best components among the L_I received components and combines them together. Figure 3.5 shows an S-Rake receiver with 5 fingers. Since the selective rake receiver has to keep track of all the replicas in order to choose the best ones, it has a higher complexity than the partial rake. The receiver complexity can be reduced by

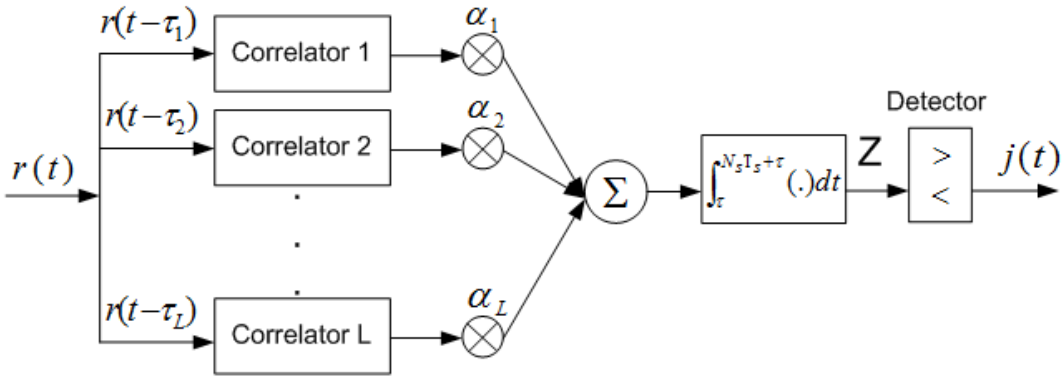

Figure 3.2: Rake receiver block diagram.

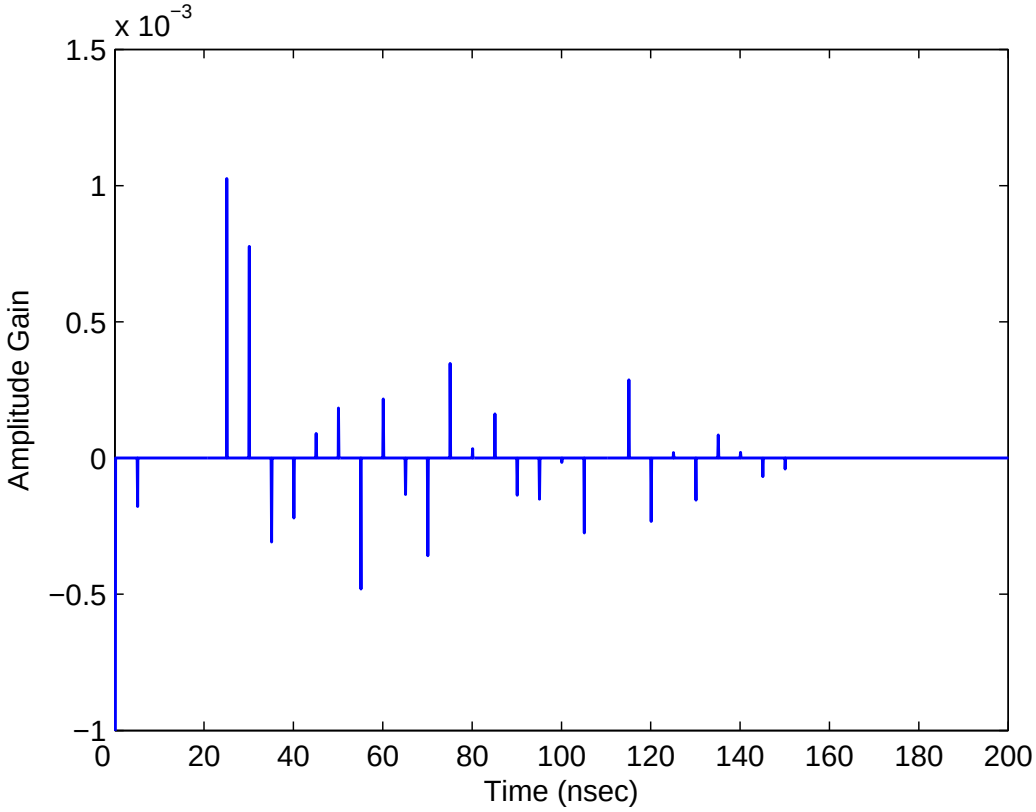

Figure 3.3: I-Rake receiver for a UWB system.

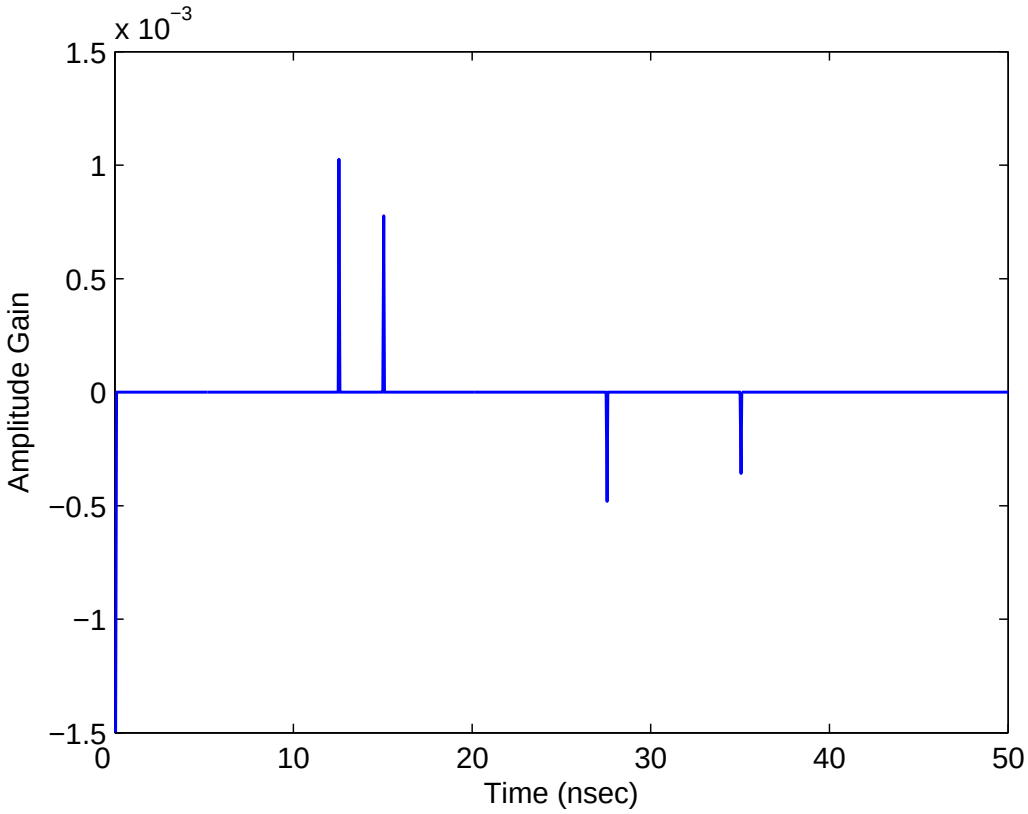

Figure 3.4: 5P-Rake receiver for a UWB system.

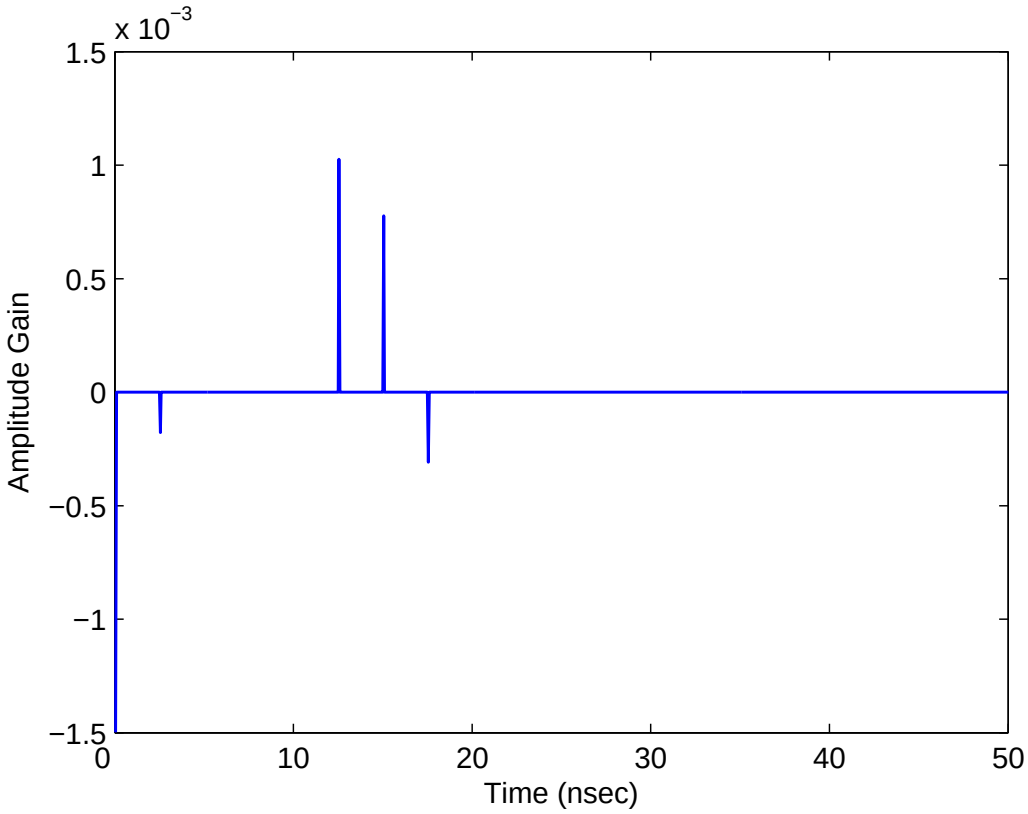

Figure 3.5: 5S-Rake receiver for a UWB system.

decreasing the number of fingers in the rake receiver. Thus, 2 finger rake receivers are given in Figs. 3.6 and 3.7. As will be shown, this lower complexity comes at the price of a performance loss.

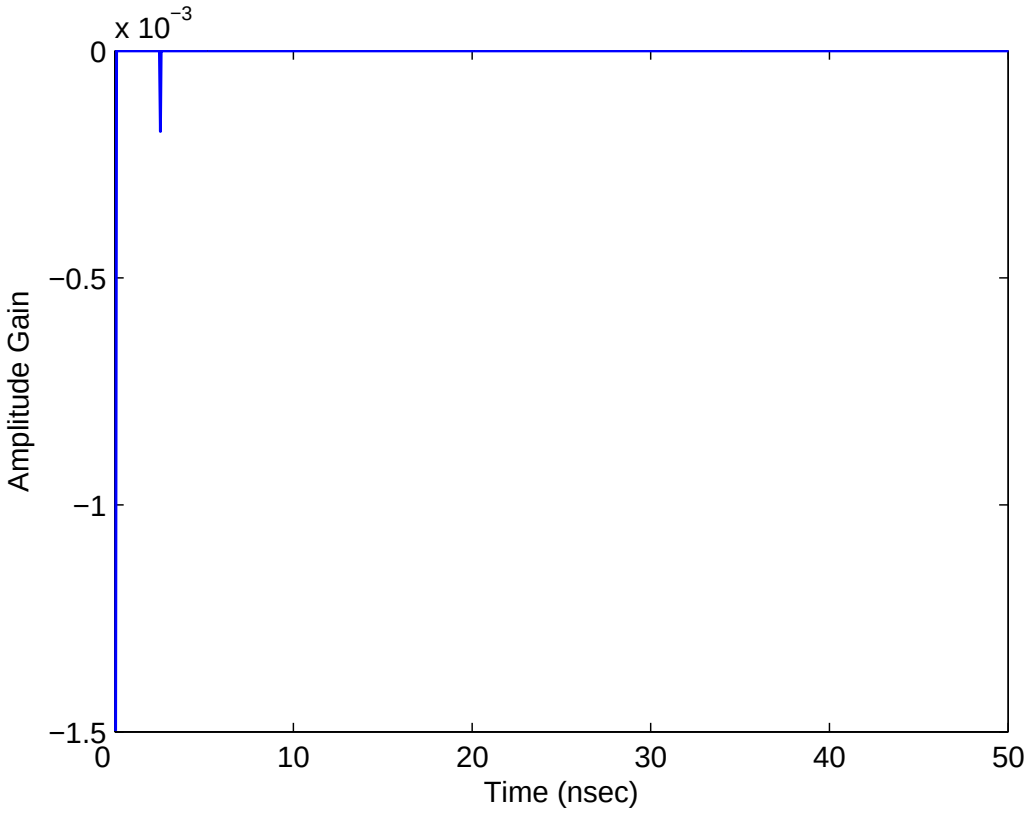

Figure 3.6: 2P-Rake receiver for a UWB system.

3.3 High Gain Directional Antenna

The 60 GHz mm-wave UWB multipath channel has high oxygen attenuation which results in a significant decrease in signal power. Also proportional to the frequency, the Doppler effects are very high at this frequency range [25]. Doppler effect or Doppler shift is the frequency change for an observer who moves toward or away from the wave source. This frequency shift is due to the difference in path lengths [20]. The high propagation loss and severe Doppler effect can be significantly reduced by using directional antennas. In addition, the performance and coverage of mm-wave can be increased with directional antennas [25].

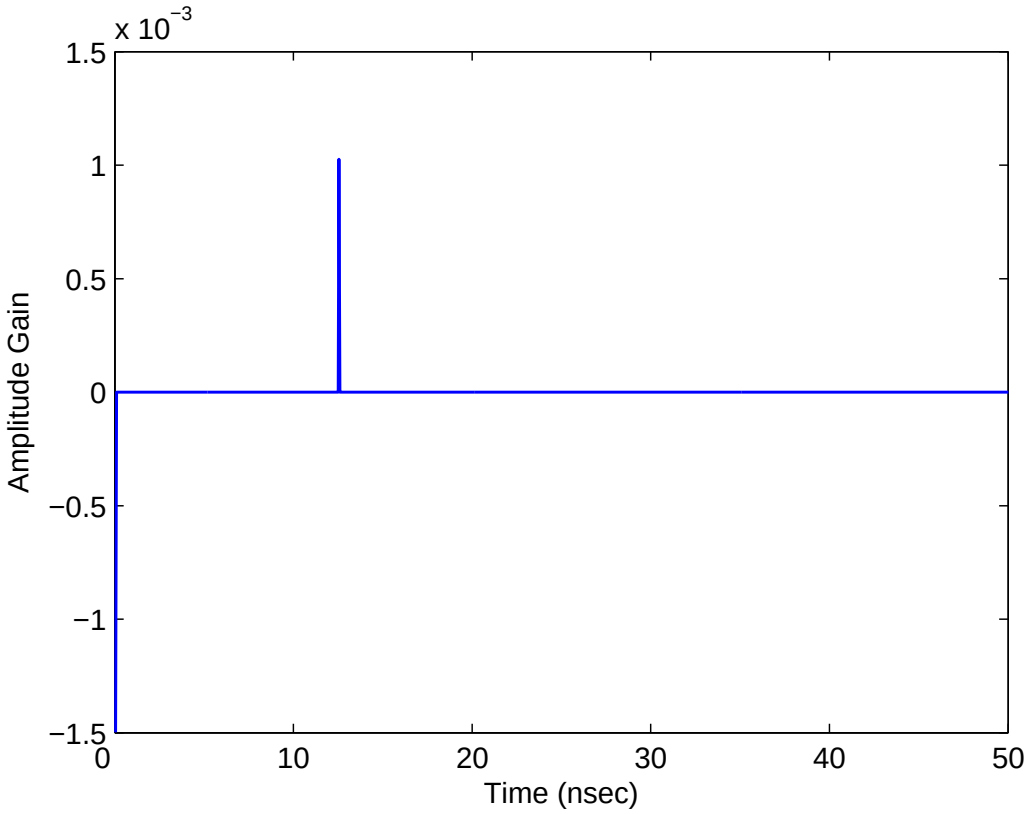

Figure 3.7: 2S-Rake receiver for a UWB system.

Directional antennas radiate the power in one direction and have higher gain than omni-directional antennas because of this narrow antenna pattern or high antenna directivity. This can improve the performance by increasing the SNR and compensate the high path loss [9]. However, problems occur in transmission with directional antennas when the LOS path is blocked by a moving object such as a human body. This problem can be overcome by using multiple antennas [26]. Fortunately, at higher frequencies, such as 60 GHz, the radio frequency (RF) components including antennas are smaller in size, which permits the use of multiple antennas [26]. The possible solutions using multiple antennas are beam steering, adaptive antenna array, antenna switching and phase array antennas [9].

Reference antenna model with average sidelobes is employed here in the simulations for the TSV channel. This is a simple mathematical model based on measured data [23]. The antenna gain for the TSV channel 2.22 based on the reference model is

$$G_r(0, \Psi_n + \psi_{nm}) = GD(0, \Psi_n + \psi_{nm}) \tag{3.18}$$

where

$$D(0, \Psi_n + \psi_{nm}) = 1$$

for omni-directional antennas, and

$$D(0, \Psi_n + \psi_{nm}) = exp(-\chi(\Psi_n + \psi_{nm})^2)$$

for directional antennas. χ represents the beam width of the antenna.

Figs. 3.8 and 3.9 show the relative antenna gain versus the angle for the transmitter and receiver. In this example, the transmitter angle is 60 degrees and the receiver angle is 15 degrees.

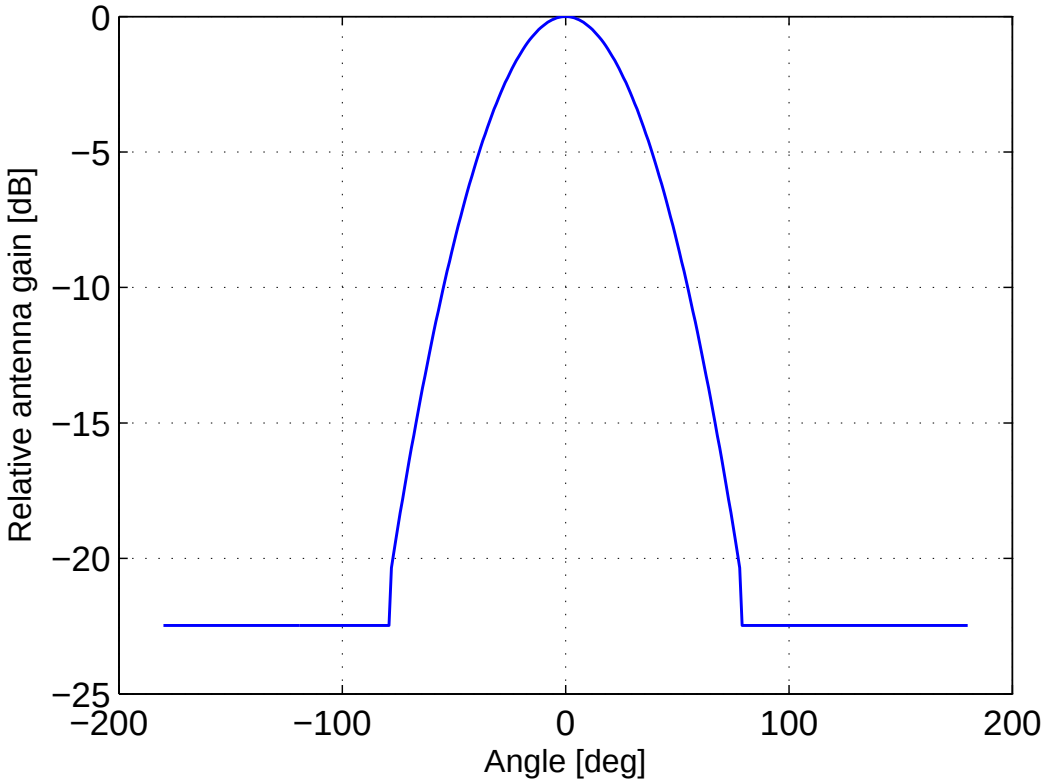

Figure 3.8: Transmitter antenna model.

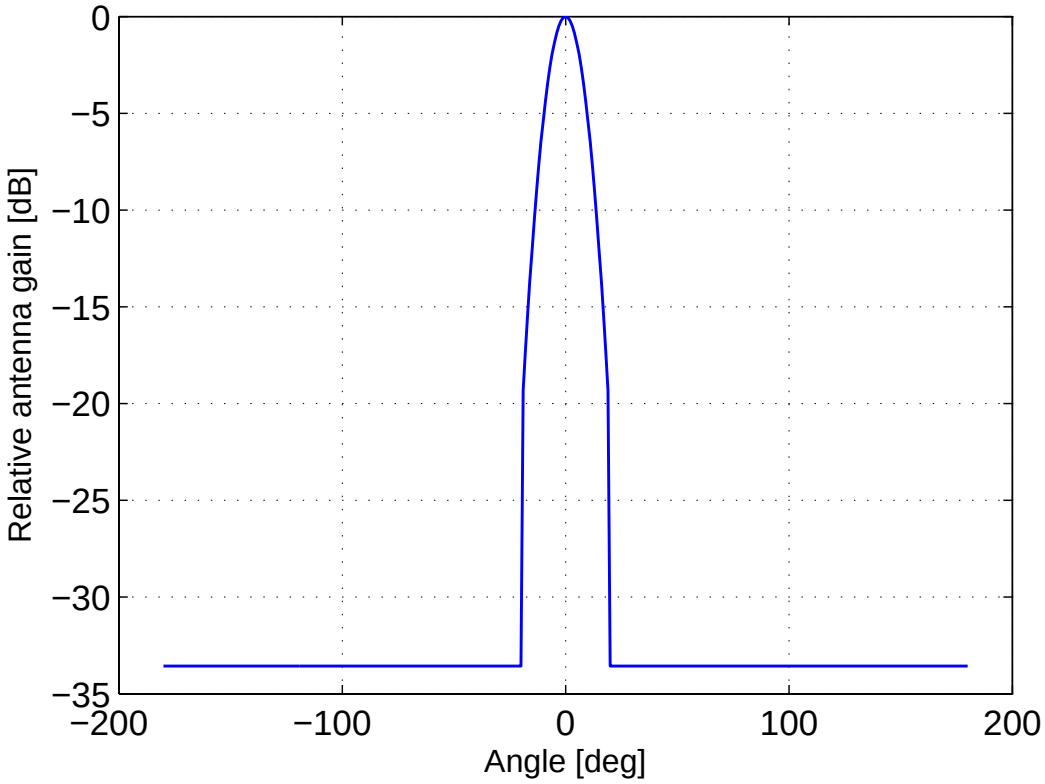

Figure 3.9: Receiver antenna model.

Chapter 4

Simulation Results

In this chapter, the bit error rate (BER) performance of orthogonal and non-orthogonal TH-PPM using the UWB channel models described in Chapter 2 is evaluated. The number of users U considered is in the range $1 \leq U \leq 16$, so the number of interferers is between 0 and 15. In addition the performance of TH-PPM over SV and TSV channels with different types of rake receiver has been compared in here.

The simulations and calculations are entirely done in Matlab. The pulse duration used in this simulation is $T_p = 0.5nsec$, the PPM time shift is $\epsilon = 0.5nsec$ and the chip time is $T_c = 1nsec$.

4.1 AWGN Channel

Figures 4.1 to 4.5 compare the performance of orthogonal and non-orthogonal TH-PPM over an AWGN channel with different numbers of interferers. With no interferers at BER = 10^{-3}, orthogonal TH-PPM outperforms non-orthogonal TH-PPM by approximately 1 dB. When the number of interferers increases to 3, orthogonal TH-PPM performs better than non-orthogonal TH-PPM up to SNR = 11 dB. For high SNRs (between 8 dB to 12 dB) with 5 interferers, non-orthogonal TH-PPM has better BER performance, and the improvement increases as the number of interferers increases. For example, with 15 interferers and SNR = 12 dB, non-orthogonal TH-PPM has BER = 4×10^{-3} dB, while orthogonal TH-PPM has BER = 4×10^{-2} for the same SNR. This shows when the number of users increases in the system, non-orthogonal PPM can achieve a better performance than the orthogonal TH-PPM. This is because by adding more interference to the users signal, orthogonal TH-PPM

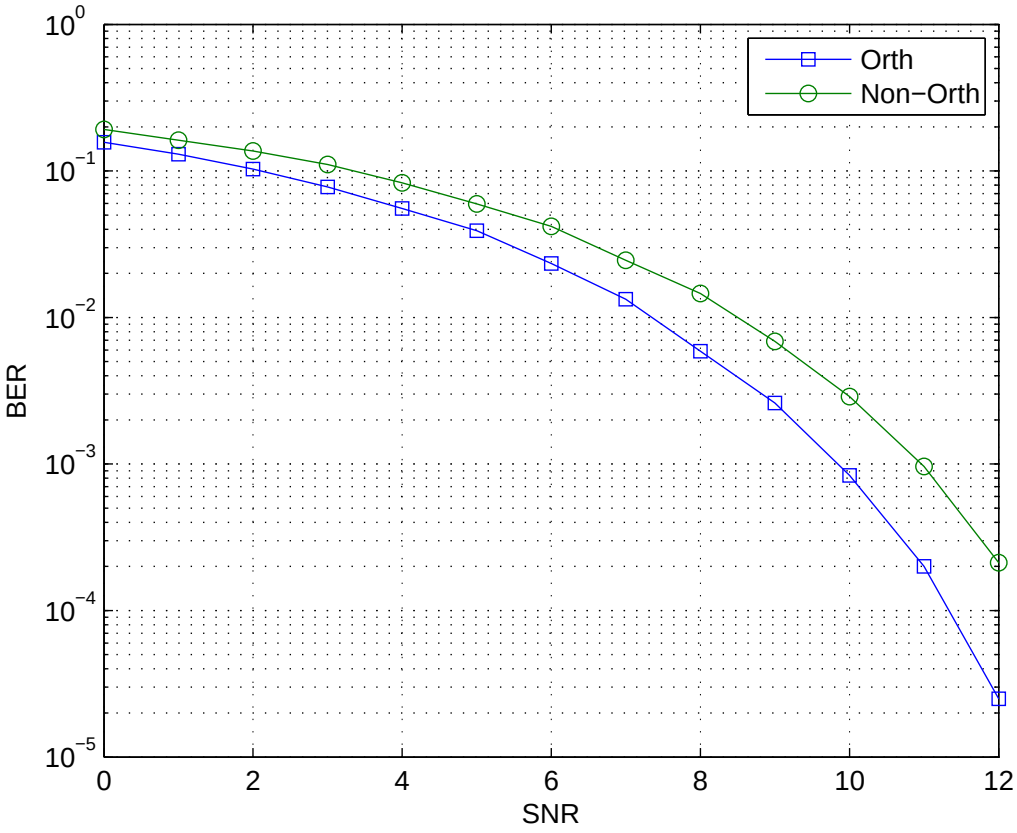

Figure 4.1: The BER performance of orthogonal and non-orthogonal TH-PPM with no interferer in AWGN Channel.

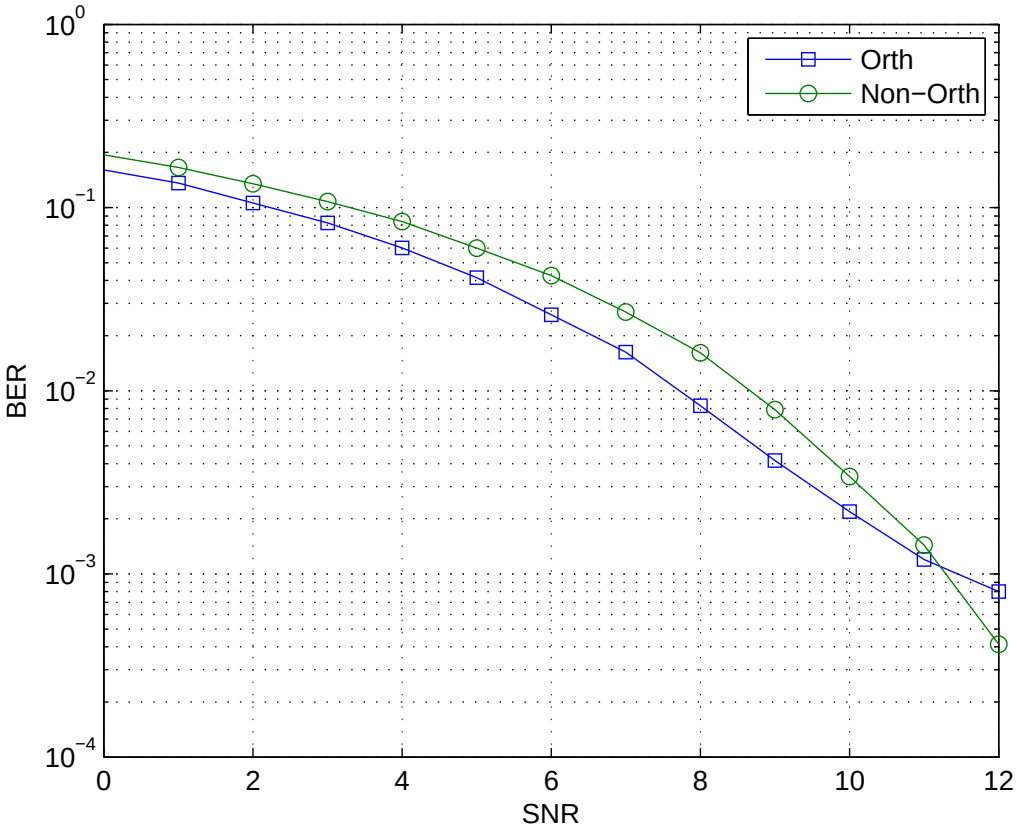

Figure 4.2: The BER performance of orthogonal and non-orthogonal TH-PPM with 3 interferers in AWGN Channel.

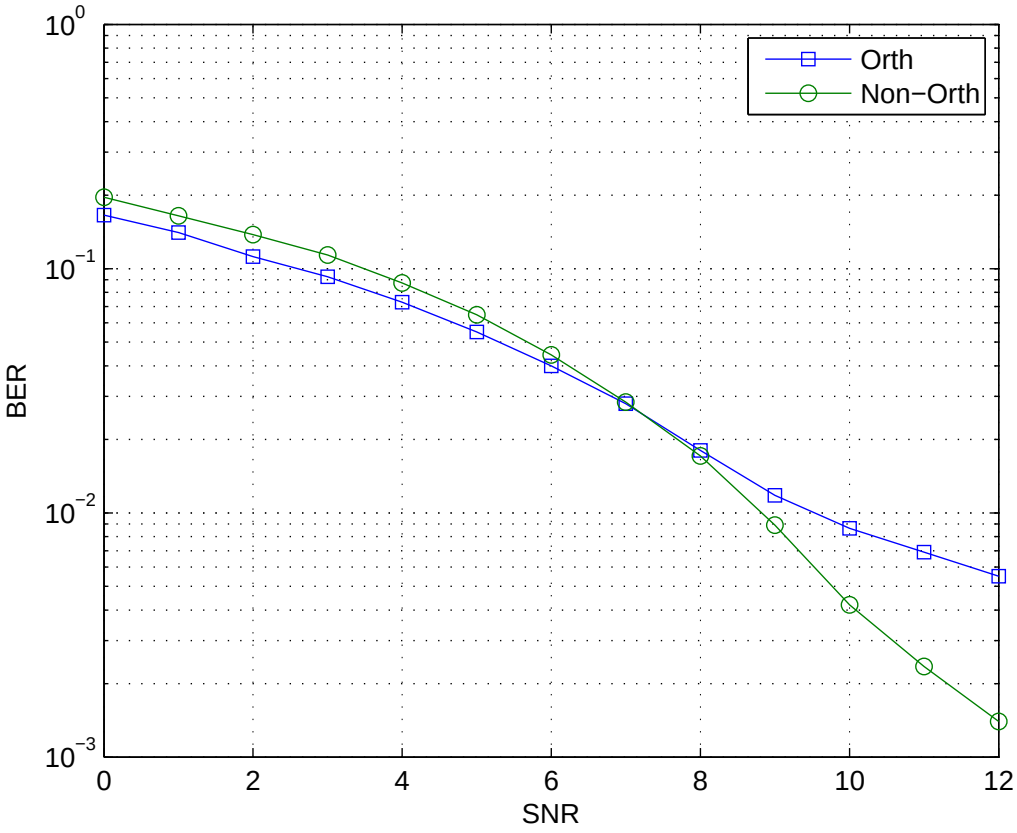

Figure 4.3: The BER performance of orthogonal and non-orthogonal TH-PPM with 5 interferers in AWGN Channel.

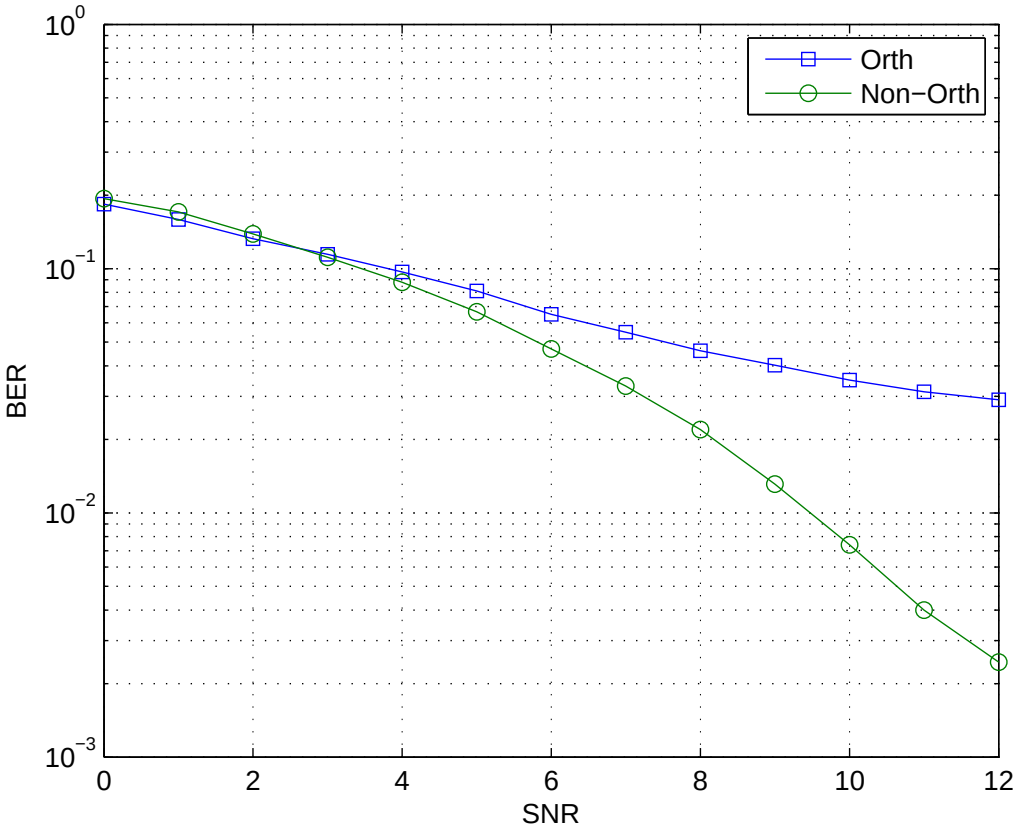

Figure 4.4: The BER performance of orthogonal and non-orthogonal TH-PPM with 10 interferers in AWGN Channel.

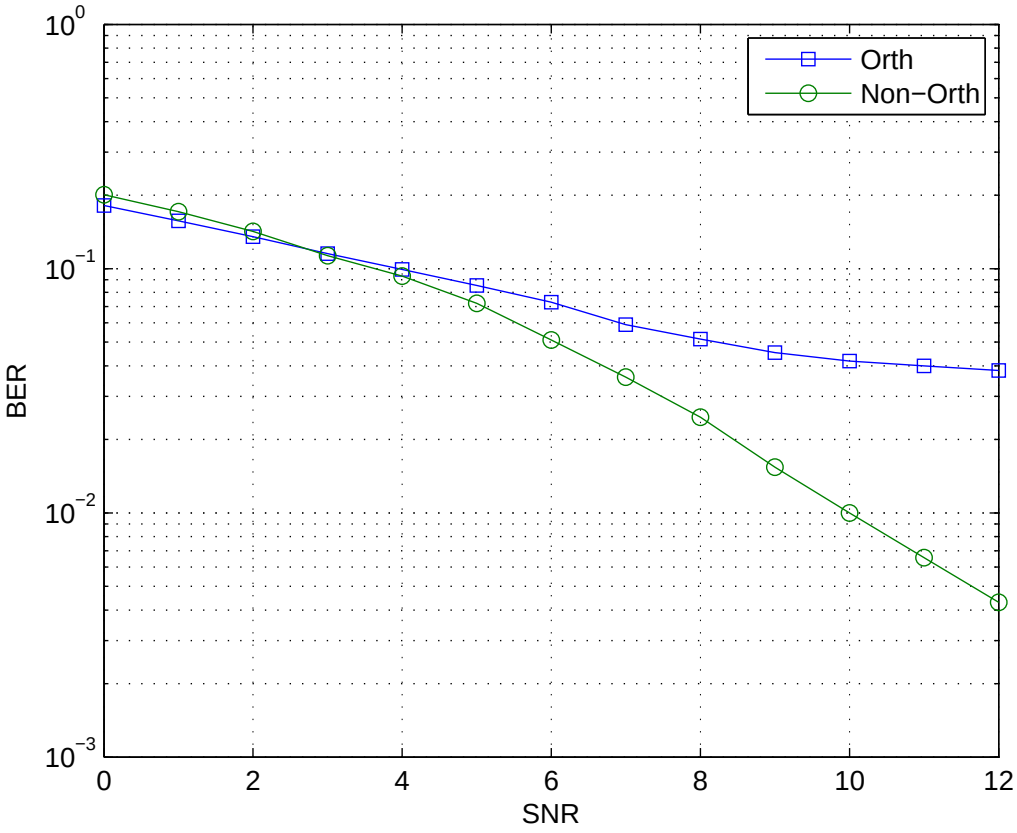

Figure 4.5: The BER performance of orthogonal and non-orthogonal TH-PPM with 15 interferers in AWGN Channel.

degrades more in compare with the non-orthogonal one, and as a result in a higher number of users involved non-orthogonal can outperform orthogonal TH-PPM.

4.2 SV Channel

In the Figure 4.6 the performance of different rake receivers on SV channel model using IEEE 802.15.3a-CM1 channel parameters has been compared. It is shown that ideal rake receiver out performs the other rakes as it contains the most number of fingers. Selective rake receiver with 5 fingers has the best performance after I-Rake receiver since it chooses the 5 strongest replicas of the signal. 5 finger partial rake receiver is however lower in performance since it chooses the first 5 replicas and not necessarily the 5 strongest. Selective and partial rake receivers with 2 fingers have the lowest performance among all. Although, ideal rake receiver has the best performance, it has a high complexity in compare with the rest of the rake receivers due to use of many fingers. Partial rake has a simpler design in compare with the selective rake since it does not need to keep track of the replicas to choose the strongest ones. As a result of this lower complexity, it can provide a lower cost receiver design.

The performance of the same signal using IEEE 802.15.3a-CM4 channel, which is the extreme NLOS case, has shown in Figure 4.7. The poor performance can be explained due to the harshness of this channel scenario. Same results is achieved as IEEE 802.15.3a-CM1 channel.

The SV channel model with parameters for the IEEE 802.15.3a-CM1 channel, which are $\Lambda = 0.0233$, $\lambda = 2.5$, $\Gamma = 7.1$, and $\gamma = 4.3$ [27], is considered here. The performance of orthogonal and non-orthogonal TH-PPM are compared in Figures 4.8 to 4.12 for this channel. This shows that the performance of both orthogonal and non-orthogonal TH-PPM degrades as the number of users increases. However, non-orthogonal TH-PPM performs better than orthogonal TH-PPM when the number of interferers is high. As an example with 5 interferers when $SNR = 9$, orthogonal and non-orthogonal TH-PPM perform the same. After that point non-orthogonal TH-PPM starts outperforming the orthogonal TH-PPM. As an example non-orthogonal TH-PPM with 10 interferers performs close to orthogonal TH-PPM with 5 interferers.

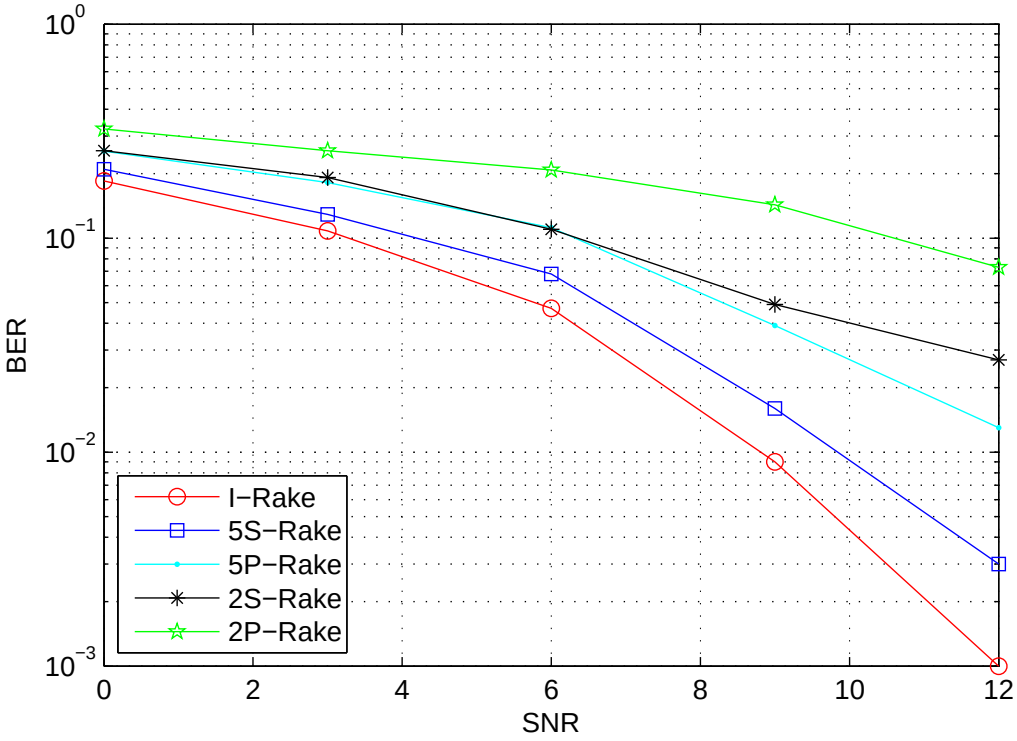

Figure 4.6: The BER Performance of TH-PPM with different rake receivers in UWB-CM1 channel

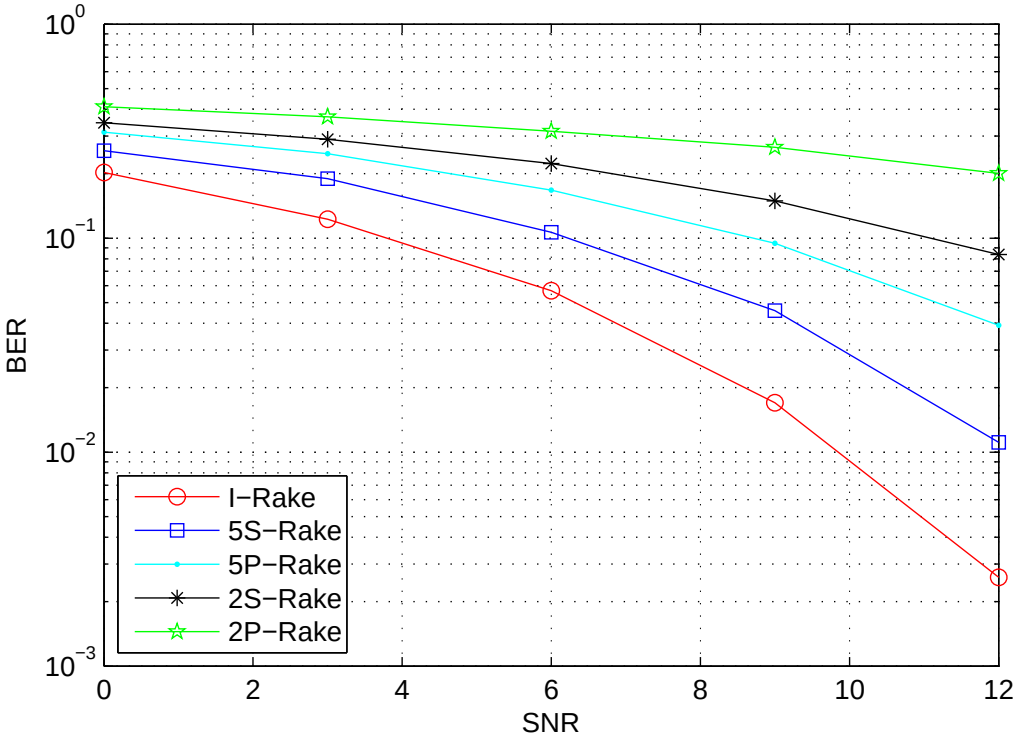

Figure 4.7: The BER Performance of TH-PPM with different rake receivers in UWB-CM4 channel

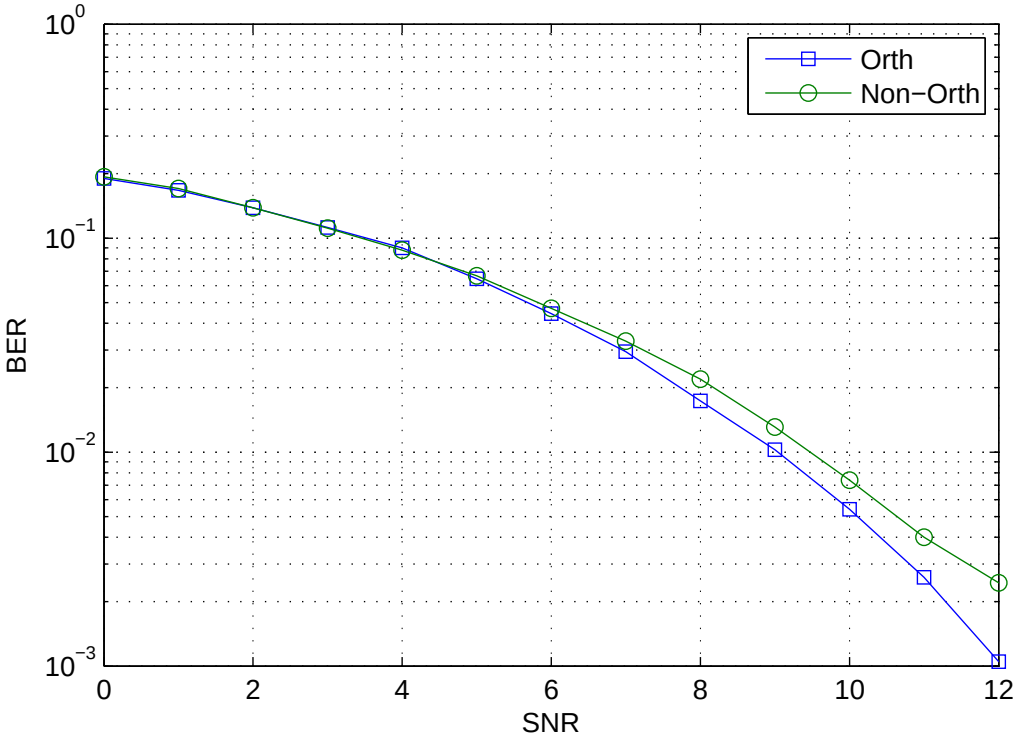

Figure 4.8: The BER performance of orthogonal and non-orthogonal TH-PPM with no interferer in SV Channel.

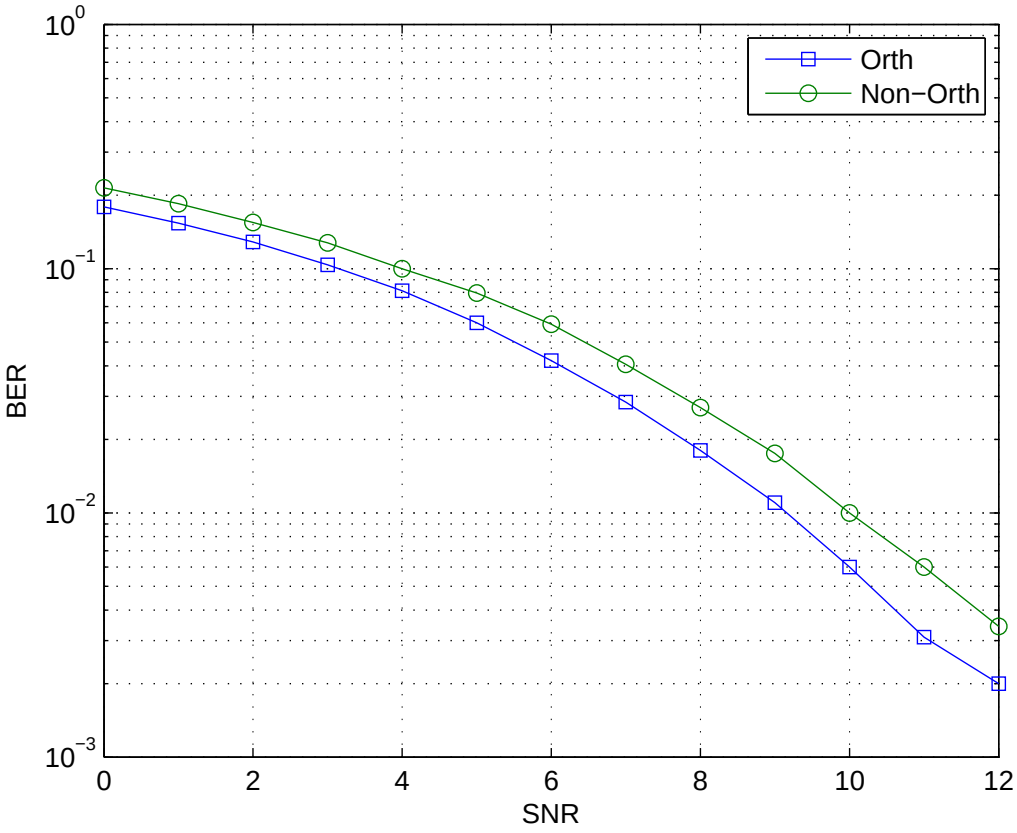

Figure 4.9: The BER performance of orthogonal and non-orthogonal TH-PPM with 3 interferers in SV Channel.

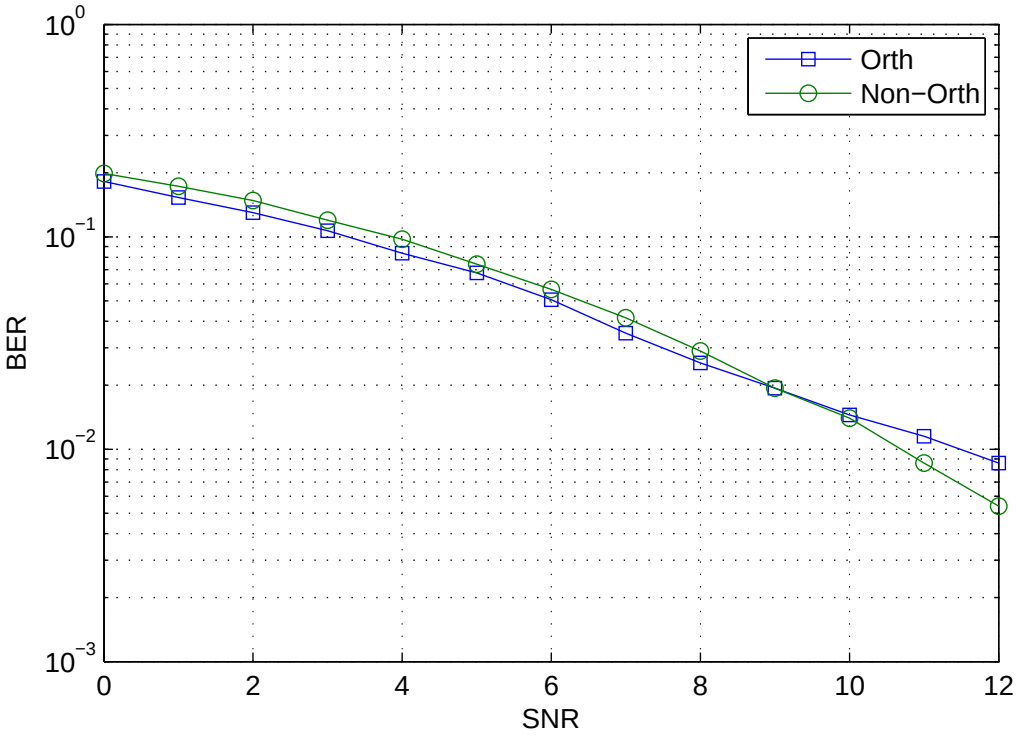

Figure 4.10: The BER performance of orthogonal and non-orthogonal TH-PPM with 5 interferers in SV Channel.

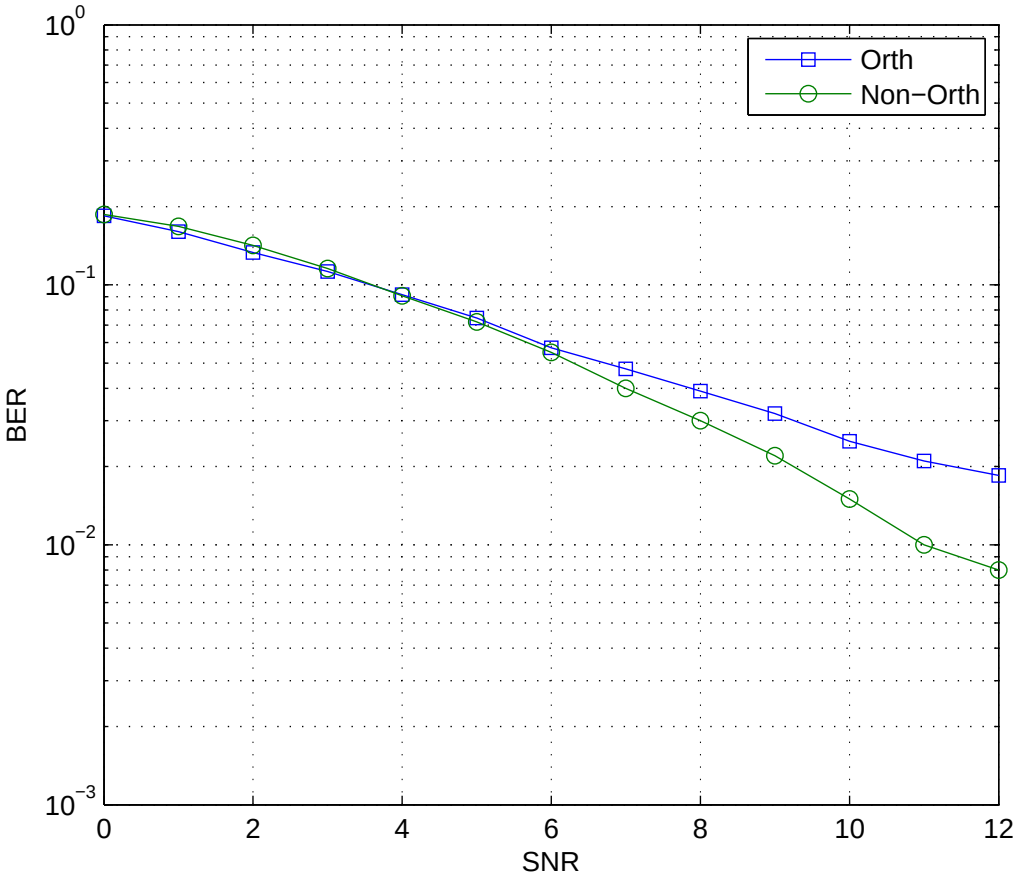

Figure 4.11: The BER performance of orthogonal and non-orthogonal TH-PPM with 10 interferers in SV Channel.

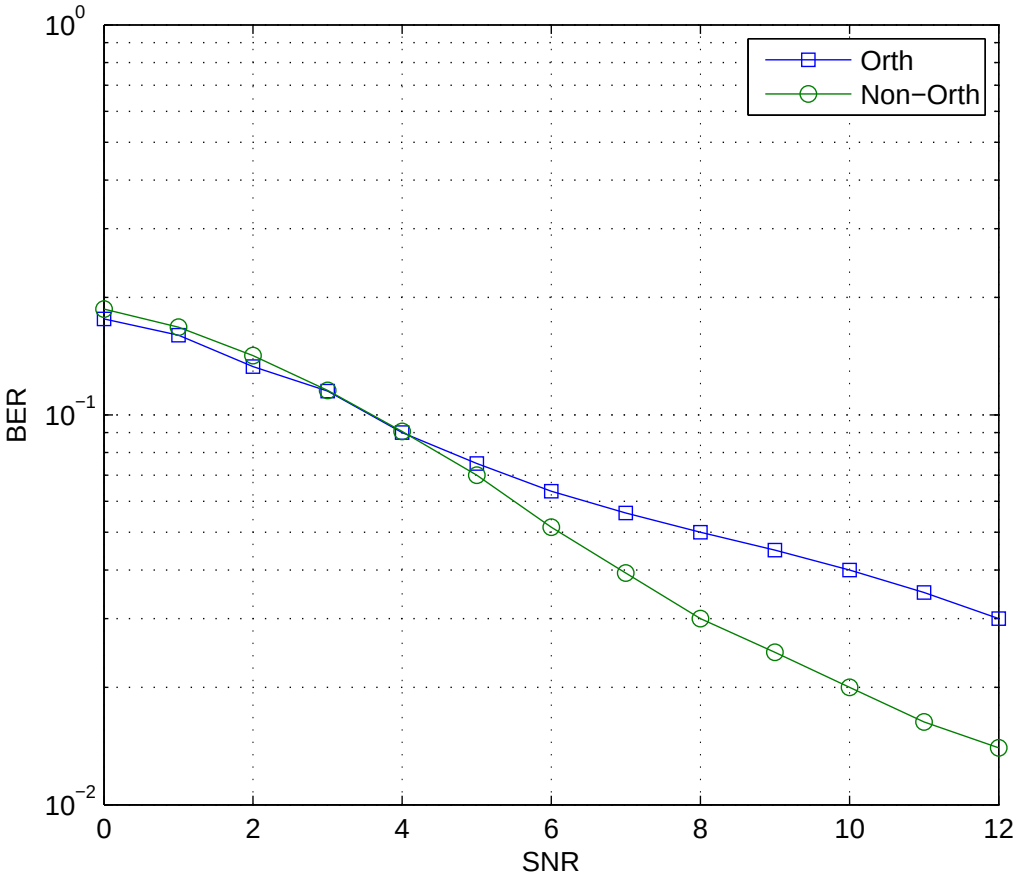

Figure 4.12: The BER performance of orthogonal and non-orthogonal TH-PPM with 15 interferers in SV Channel.

4.3 TSV Channel

For the TSV channel model, the IEEE 802.15.3c-CM1.1 channel with $\Lambda = 0.191$, $\lambda = 1.22$, $\Gamma = 4.46$, and $\gamma = 6.25$ [23], is considered. Directional antennas have been used with angles of 360 and 15 degrees for the transmitter and receiver, respectively.

Figures 4.13 to 4.17 show the performance of orthogonal and non-orthogonal TH-PPM with different numbers of interferers. As with the previous channels, an increase in the number of users increases the BER with both modulation techniques. Same as SV channel in here also non-orthogonal TH-PPM has better performance than orthogonal TH-PPM when the number of users is large.

Comparing Figures 4.13 to 4.17 to the ones in SV channel, the performance with both orthogonal and non-orthogonal TH-PPM in the TSV channel model is close to that with the SV channel model. Even though TSV channel model has a severe attenuation and higher path loss than the lower frequency band channels [8], TH-PPM modulation can achieve similar performance in both channel models. This shows the robustness of TH-PPM modulation scheme in UWB channels.

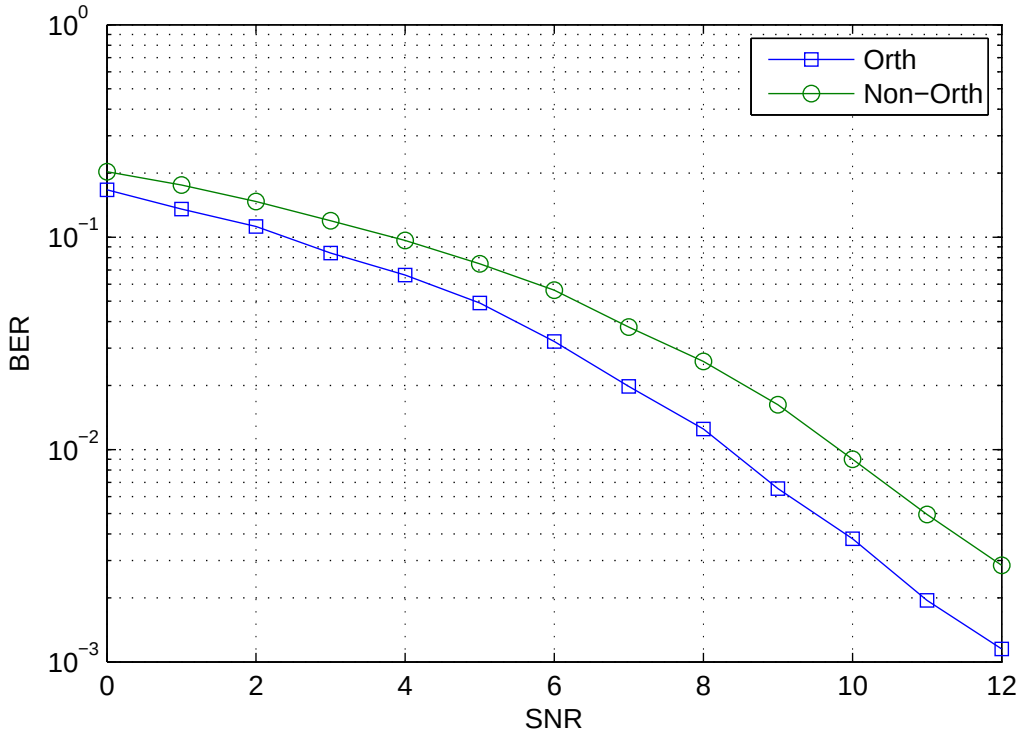

Figure 4.13: The BER performance of orthogonal and non-orthogonal TH-PPM with no interferer in TSV Channel.

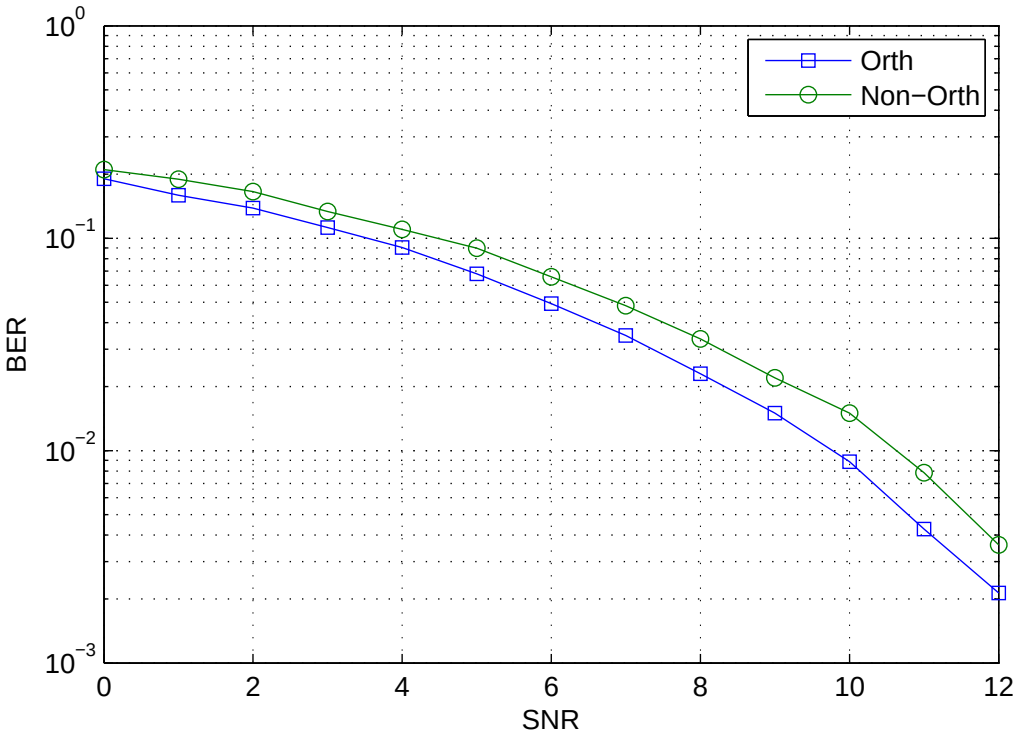

Figure 4.14: The BER performance of orthogonal and non-orthogonal TH-PPM with 3 interferers in TSV Channel.

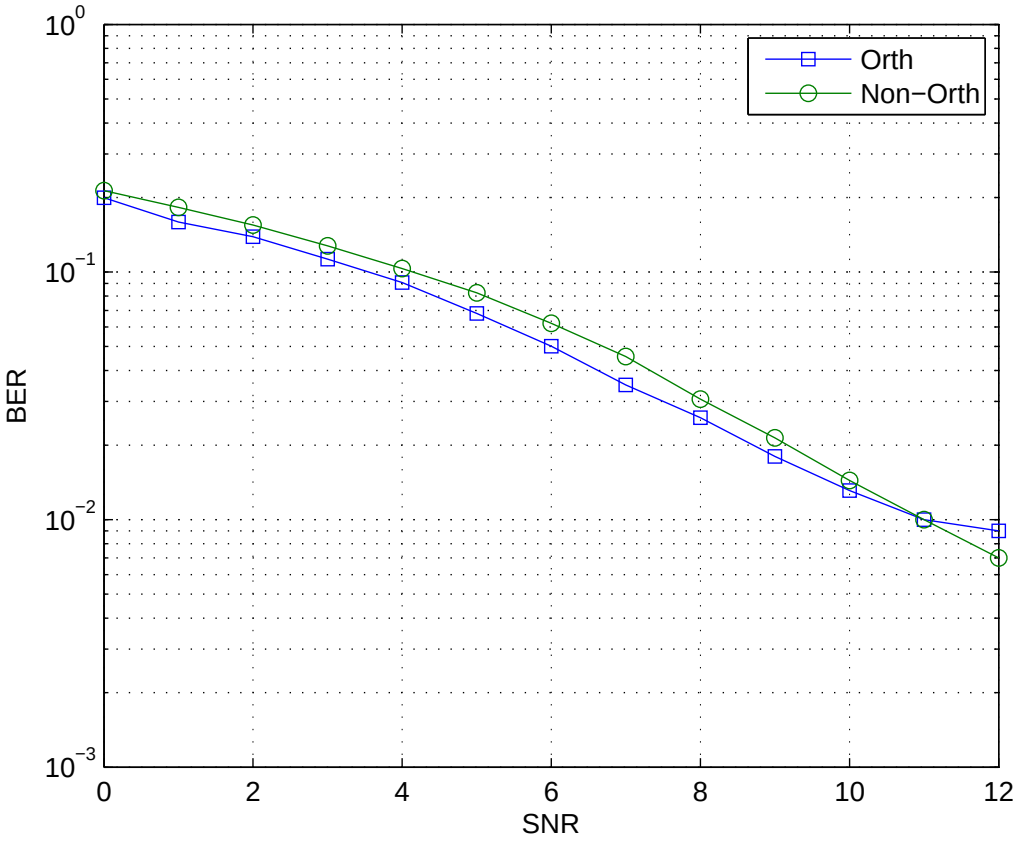

Figure 4.15: The BER performance of orthogonal and non-orthogonal TH-PPM with 5 interferers in TSV Channel.

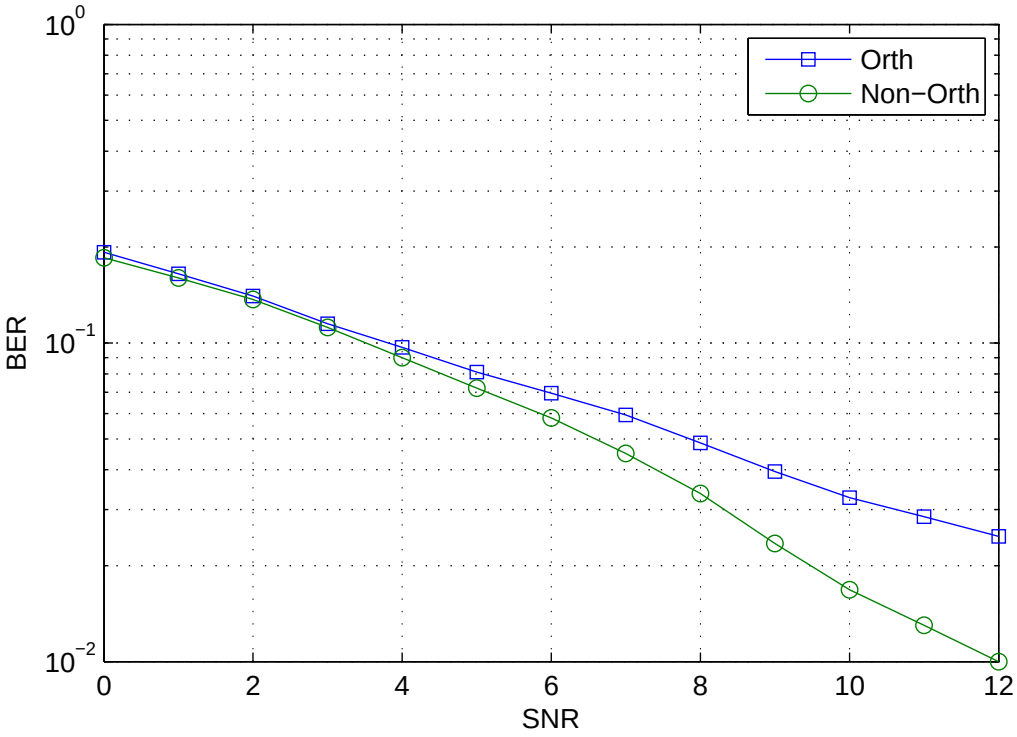

Figure 4.16: The BER performance of orthogonal and non-orthogonal TH-PPM with 10 interferers in TSV Channel.

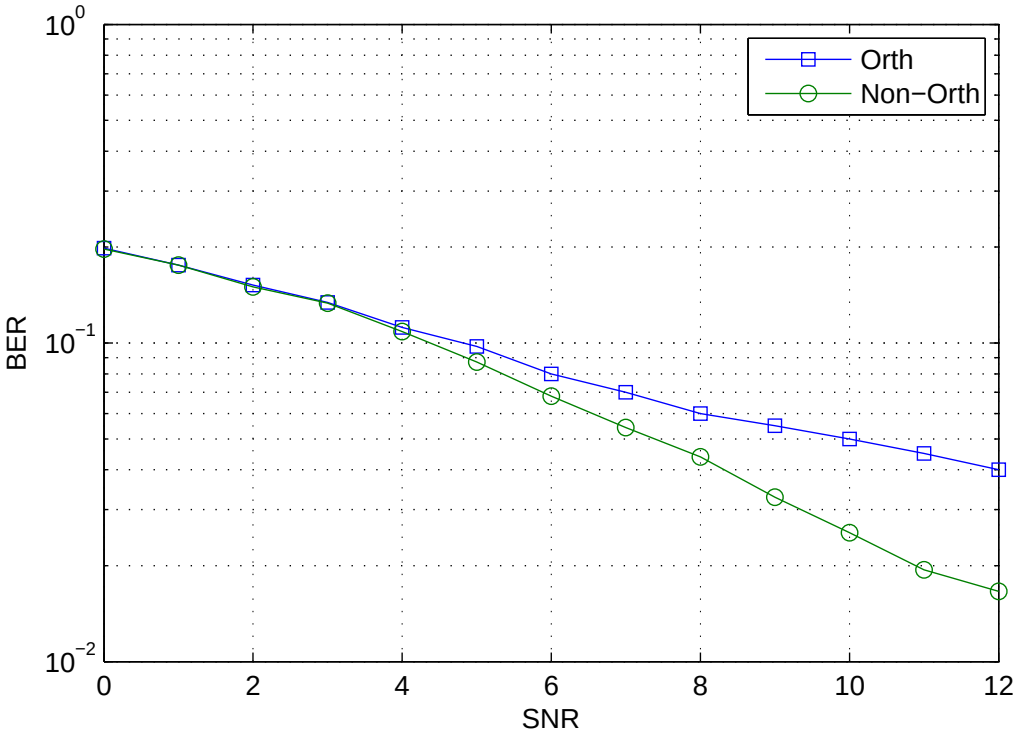

Figure 4.17: The BER performance of orthogonal and non-orthogonal TH-PPM with 15 interferers in TSV Channel.

Chapter 5

Conclusions and Future Work

5.1 Conclusions

Ultra wideband (UWB) is a promising way of communications which provides a very fast and secure connection between transmitter and receiver. Systems required high bandwidth, low power consumption and shared frequency spectrum resources can take advantage of this technology. In multipath environments UWB can provide secure and low interference connections. Because of the tradeoff between data rate and distance, UWB can be applied to several different wireless applications.

Different types of modulations can be used for UWB such as on-off keying (OOK), pulse amplitude modulation (PAM), pulse position modulation (PPM) and pulse position amplitude modulation (PPAM). PPM was chosen for this thesis and time hopping (TH) was applied to reduce the interference in multiple access environments. Higher frequency UWB, 60 GHz mm-wave, was introduced as lower frequency UWB is not globally available and because mm-wave UWB can support applications which require a higher data rate.

The bit error rate (BER) performance of orthogonal and non-orthogonal time hopping pulse position modulation (TH-PPM) has been evaluated for ultra wideband (UWB) communication systems. Two channel models, Saleh-Valenzuela (SV) and triple-SV (TSV) were considered with various numbers of users. The SV channel is a typical channel model used for the 3.1 - 10.6 GHz UWB band, while the TSV channel corresponds to the 60 GHz millimeter wave (mm-wave) UWB band.

It was shown that the number of users has a significant impact on the performance of both orthogonal and non-orthogonal TH-PPM. However, non-orthogonal TH-PPM

provides better performance when the number of users is large. The performance of orthogonal and non-orthogonal TH-PPM modulation in the TSV channel is similar to that in the SV channel. This shows that TH-PPM modulation is a good candidate for UWB communications since it can provide good performance even in multipath fading, which shows the robustness of this modulation scheme. In addition, the performance of different rake receivers has been compared for the SV channel model. While the ideal rake has the best performance, it is not practical to have a rake receiver with this many fingers due to the high complexity of the receiver. It was shown that a selective rake receiver with 5 fingers outperforms the other receivers that were considered. A partial rake receiver, on the other hand, has a simpler design in comparison with selective rake since it does not have to keep track of the signal replicas to choose the strongest ones. As a result, it can provide a lower cost receiver at the expense of reduced performance. Directional antennas were considered for TSV channel model. The directivity helps mm-wave UWB systems combat the Doppler effects caused by moving objects.

5.2 Future Work

In this thesis TH-PPM modulation using both orthogonal and non-orthogonal pulses was introduced. The performance was evaluated for AWGN, SV and TSV models. It was shown that non-orthogonal TH-PPM has better performance than orthogonal TH-PPM when the number of users is large. The results are the same for all the channels considered.

As PPM is the only modulation employed in this thesis, this work can be extended to other modulation schemes such as PAM and PPAM with a variety of pulse shapes. Sine, first and second derivative Gaussian, and rectangular pulse shapes can be employed since they all satisfy the FCC's spectral mask requirements. The second derivative of the Gaussian pulse was used in this thesis.

Different channel models can also be considered. The SV and TSV models are the two most commonly used channels have been approved by IEEE. However, many other channel models have been proposed for UWB and mm-wave UWB communications.

Within the SV and TSV channel models, several scenarios exist which can be used depending on the environment. These scenarios include residential, office, desktop, and kiosk environments with LOS and NLOS signal paths. A residential scenario was used here. Thus these other scenarios would be useful to investigate in the future.

Bibliography

[1] R. A. Scholtz, "Multiple access with time-hopping impulse modulation," *Proc. IEEE Military Commun. Conf.*, pp. 11–14, Oct 1993.

[2] M. Z. Win and R. A. Scholtz, "Impulse radio: How it works," *IEEE Commun. Lett.*, vol. 2, pp. 36–38, Feb 1998.

[3] F. Nekoogar, *Ultra-wideband Communications: Fundamentals and Applications*. Prentice Hall, 2005.

[4] I. Oppermann, M. Hamalainen, and J. Iinatti, *UWB Theory and Applications*. Wiley, 2004.

[5] Federal Communications Commission, "Revision of Part 15 of the Commission's rules regarding ultra-wideband transmission systems," *FCC 02-48*, Apr 2002.

[6] B. Sklar, *Digital Communications: Fundamentals and Applications*. Prentice Hall, 2nd ed., 2001.

[7] R. C. Daniels and R. W. Heath, "60 GHz wireless communication: Emerging requirements and design recommendations," *IEEE Vehic. Tech. Magazine*, vol. 2, pp. 41–50, Sept 2007.

[8] C. Park and T. S. Rappaport, "Short-range wireless communications for next-generation networks: UWB, 60 GHz millimeter-wave WPAN, and ZigBee," *IEEE Trans. Wireless Commun.*, vol. 14, pp. 70–78, Aug 2007.

[9] N. Guo, R. C. Qiu, S. S. Mo, and K. Takahashi, "60 GHz millimeter-wave radio: Principle, technology, and new results," *EURASIP J. on Wireless Commun. and Networking*, p. 8, Sept 2006.

[10] K. A. Hamidi and X. Gu, "On the validity of the Gaussian approximation for performance analysis of TH-CDMA/OOK impulse radio networks," *Proc. IEEE Vehic. Tech. Conf.*, pp. 2211–2215, Apr 2003.

[11] Z. Bai and K. Kwak, "Analysis of multiuser DS-PAM and TH-PPM UWB systems in data and image transmission," *Proc. IEEE Int. Conf. on Wireless Commun., Networking and Mobile Computing*, pp. 324–327, Sept 2005.

[12] H. Zhang, W. Li, and T. A. Gulliver, "Pulse position amplitude modulation for time-hopping multiple-access UWB communications," *Proc. IEEE Wireless Commun. and Networking Conf.*, pp. 895–900, Mar 2004.

[13] Y. P. Zhang, M. Sun, K. M. Chua, L. L. Wai, D. Liu, and B. P. Gaucher, "Antenna-in-package in LTCC for 60 GHz radio," *Proc. Int. Workshop on Antenna Technology: Small and Smart Antennas Metamaterials and Applications*, pp. 279–282, Mar 2007.

[14] X. Chen and S. Kiaei, "Monocycle shapes for ultra wideband system," *Proc. IEEE Int. Symp. on Circuits and Systems*, pp. 597–600, May 2002.

[15] H. Xie, X. Wang, A. Wang, B. Qin, H. Chen, Y. Zhou, and B. Zhao, "A varying pulse width second order derivative gaussian pulse generator for UWB transceivers in CMOS," *Proc. IEEE Int. Symp. on Circuits and Systems*, pp. 2794–2797, May 2007.

[16] M. D. Benedetto and B. R. Vojcic, "Ultra wide band wireless communications: A tutorial," *J. Commun. and Networks*, vol. 5, pp. 290–302, Dec 2003.

[17] H. Zhang, W. Li, and T. A. Gulliver, "Performance analysis of non-orthogonal pulse position modulation for time-hopping UWB transmission," *Proc. IEEE Commun. Networks and Services Research Conf.*, pp. 287–293, May 2007.

[18] A. A. M. Saleh and R. A. Valenzuela, "A statistical model for indoor multipath propagation," *IEEE J. Select. Areas Commun.*, vol. 5, pp. 128–137, Feb 1987.

[19] G. L. Turin, F. D. Clapp, T. L. Johnston, S. B. Fine, and D. Lavry, "A statistical model of urban multipath propagation," *IEEE Trans. Vehic. Tech.*, vol. 21, no. 1, pp. 1–9, 1972.

[20] T. S. Rappaport, *Wireless Communications: Principles and Practice*. Prentice Hall, 2nd ed., 2001.

[21] H. Sawada, Y. Shoji, and C. S. Choi, "Proposal of novel statistic channel model for millimeter wave WPAN," *Proc. Asia-Pacific Microwave Conf.*, pp. 1855–1858, Dec 2006.

[22] S. Promwong, J. Takada, P. Supanakoon, and P. Tangtisanon, "Theoretical ground reflection model for UWB communication systems," *Proc. Int. Sym. Commun. and Information Tech.*, pp. 1208–1212, Oct 2004.

[23] http://ieee802.org/15/pub/TG3c.html

[24] M. Benedetto and G. Giancola, *Understanding Ultra Wide Band Radio Fundamentals*. Prentice Hall, 2004.

[25] H. Yang, P. F. M. Smulders, and M. H. A. J. Herben, "Channel characteristics and transmission performance for various channel configurations at 60 GHz," *EURASIP J. on Wireless Commun. and Networking*, p. 15, Mar 2007.

[26] S. K. Yong and C.-C. Chong, "An overview of multi gigabit wireless through millimeter wave technology: Potentials and technical challenges," *EURASIP Journal on Wireless Commun. and Networking*, p. 8, Sept 2006.

[27] http://ieee802.org/15/pub/TG3a.html